Publications of the Astronomical Society of Australia (2025), **42**, e037, 16 pages
doi:10.1017/pasa.2025.12

CAMBRIDGE UNIVERSITY PRESS

Research Article

Long-term spin-down and low luminosity regime in the Be/X-ray binary pulsar GX 304-1

Amar Deo Chandra
Aryabhatta Research Institute of Observational Sciences, Manora Peak, Nainital, Uttrakhand, India

Abstract

We carry out timing and spectral studies of the Be/X-ray binary pulsar GX 304-1 using *NuStar* and *XMM-Newton* observations. We construct the long-term spin period evolution of the pulsar which changes from a long-term spin-up ($\sim 1.3 \times 10^{-13}$ Hz s^{-1}) to a long-term spin-down ($\sim -3.4 \times 10^{-14}$ Hz s^{-1}) trend during a low luminosity state ($\sim 10^{34-35}$ erg s^{-1}). A prolonged low luminosity regime ($L_X \sim 10^{34-35}$ erg s^{-1}) was detected during 2005–2010 and spanning nearly five years since 2018 December. The *XMM-Newton* and *NuStar* spectra can be described with a power law plus blackbody model having an estimated luminosity of $\sim 2.5 \times 10^{33}$ and $\sim 3.6 \times 10^{33}$ erg s^{-1}, respectively. The inferred radius of the blackbody emission is about 100–110 m which suggests a polar-cap origin of this component. From long-term ultraviolet observations of the companion star, an increase in the ultraviolet signatures is detected preceding the X-ray outbursts. The spectral energy distribution of the companion star is constructed which provides a clue of possible UV excess when X-ray outbursts were detected from the neutron star compared to the quiescent phase. We explore plausible mechanisms to explain the long-term spin-down and extended low luminosity manifestation in this pulsar. We find that sustained accretion from a cold disc may explain the prolonged low luminosity state of the pulsar since December 2018 but the pulsar was undergoing normal accretion during the low luminosity period spanning 2005–2010.

Keywords: Accretion; accretion discs; stars: mass-loss; stars: neutron; pulsars: individual: GX 304-1; stars: winds, outflows; X-rays: binaries

(Received 23 September 2024; revised 17 January 2025; accepted 23 January 2025)

1. Introduction

The Be/X-ray binary (BeXRB) pulsar GX 304-1 was first detected using balloon-borne observations in 1967 (McClintock, Ricker, & Lewin 1971). It was subsequently detected using *Uhuru* observations and listed in the *Uhuru* catalogue (Giacconi et al. 1974). X-ray pulsations having a periodicity of about 272 s were detected from this source using *SAS-3* observations (McClintock et al. 1977). Similar pulsation period was inferred using *Ariel V* observations of the source (Huckle et al. 1977). Spectral investigations of the pulsar were performed using follow-up observations (Maurer et al. 1982; White, Swank, & Holt 1983), and the spectrum was found to be hard ($\Gamma \sim 2$) and described using an absorbed power law. The orbital period of the binary was estimated to be about 132.5 d from modulations in the X-ray outbursts from *Vela 5B* observations (Priedhorsky & Terrell 1983). The optical companion of the binary pulsar was identified by Bradt et al. (1977). The companion star V850 Cen was found to be of B2Vne type using optical observations (Mason et al. 1978; Thomas, Morton, & Murdin 1979; Parkes, Murdin, & Mason 1980), and photometric studies of the companion star were carried out (Menzies 1981). The distance of the source was estimated to be 2.4 ± 0.5 kpc by Parkes et al. (1980) and recent *Gaia* observations pin down the distance to 2.01 ± 0.15 kpc (Treuz et al. 2018). The pulsar was not detected using *EXOSAT* monitoring observations in 1984 July/August which suggested that the source was in an 'off' state (Pietsch et al. 1986). The putative cause of this intriguing 'off' state was attributed to the loss in the decretion disc around the companion star from long-term optical observations (Pietsch et al. 1986; Corbet et al. 1986).

The pulsar lay dormant for about three decades until 2008 when it was detected using *INTEGRAL* (Manousakis et al. 2008) and regular outbursts spaced by the orbital period were detected until mid-2013 (Yamamoto et al. 2009; Mihara et al. 2010; Krimm et al. 2010; Nakajima et al. 2010; Kühnel et al. 2010; Yamamoto et al. 2011b,c, Yamamoto et al. 2012). The orbital period was refined to 132.1885 ± 0.022 d using *MAXI* observations of the recurrent outbursts (Sugizaki et al. 2015). The pulsation period detected during the 2010 August period was about 275.4 s which suggested that the pulsar had spun down by about 3 s during the quiescent period lasting for about 28 yr (Devasia et al. 2011; Yamamoto et al. 2011a). A cyclotron absorption feature at around 54 keV was detected in the spectrum using *RXTE* observations during the 2010 August outburst (Yamamoto et al. 2011a) which was confirmed using *INTEGRAL* observations of the source (Klochkov et al. 2012). The pulsar remained quiescent until a weak X-ray brightening was detected in 2016 January (Nakajima et al. 2016b) and then in 2016 May (Nakajima et al. 2016a; Sguera & Sidoli 2016; Rouco Escorial & Wijnands 2016). Thereafter, the pulsar lay in a low luminosity state and accretion-induced pulsations were detected from the pulsar using *NuStar* observations of the source during a low luminosity state in 2018 June which was suggested to occur from a cold disc (Escorial, van den Eijnden, & Wijnands 2018). The pulsar lay in an enigmatic low luminosity

Corresponding author: Amar Deo Chandra; Email: amar.deo.chandra@gmail.com.

Cite this article: Chandra AD. (2025) Long-term spin-down and low luminosity regime in the Be/X-ray binary pulsar GX 304-1. *Publications of the Astronomical Society of Australia* **42**, e037, 1–16. https://doi.org/10.1017/pasa.2025.12

state for almost a year from around 2017 September, wherein the *Swift*/X-ray Telescope (XRT) count rate varied by a factor of only ∼2-3 and was not tied to any particular orbital phase (Escorial et al. 2018). This peculiar behaviour was not well understood and was surmised to be due to accretion from a cold disc (Escorial et al. 2018).

In this paper, we investigate the long-term spin period evolution and low luminosity regime of GX 304-1 using multi-wavelength observations. The paper is organised as follows. We describe observations from the *NuStar*, the *XMM-Newton* and the *Swift* missions and their data analysis procedures in Section 2. In Section 3, we carry out timing and spectral studies using *NuStar* and *XMM-Newton* observations and construct the long-term spin evolution of the pulsar. This is followed by exploring the X-ray activity of the pulsar during the period when the spin evolution of the pulsar was surmised to have changed from a long-term spin-up to a long-term spin-down trend. The long-term photometric and ultraviolet observations of the companion star are explored. Thereafter, we study the long-term low-level X-ray activity of the pulsar using archival *Neil Gehrels Swift Observatory* observations. In Section 4, we discuss possible mechanisms that can lead to a long-term spin-down in the pulsar and sustained low luminosity manifestation of the pulsar. In addition, we also probe the origin of soft X-ray excess in the low luminosity spectra of the neutron star and explore the spectral energy distribution of the companion star. We summarise our findings in Section 5.

2. Observations and data reduction

We analyse unpublished *NuStar* and *XMM-Newton* observations of GX 304-1 from 2022 January and 2023 July, respectively. The source was observed on several occasions during regular outbursts and quiescent phases using the *Neil Gehrels Swift Observatory* since 2005 April. The X-ray activity of the pulsar during the period 2012 January 1 until 2018 October 30 was explored by Escorial et al. (2018) using the X-ray Telescope (XRT) onboard the *Neil Gehrels Swift Observatory*. We explore the X-ray activity of the pulsar using unpublished *Swift*/XRT observations from 2005 April 6–2010 March 15 and 2018 December 17–2024 February 27.

2.1 NuStar observation

The *Nuclear Spectroscopic Telescope Array* (*NuStar*) is a hard X-ray telescope consisting of two identical modules (FPMA and FPMB) operating in the energy range 3–79 keV (Harrison et al. 2013). *NuStar* observed GX 304-1 on 2022 January 29 (MJD 59608.5, ObsID 30701015002) for a total duration of about 174 ks. Fig. 1 shows the one-day averaged monitoring observations of GX 304-1 from the *MAXI* mission in the 2–20 keV energy band and the epoch of the *NuStar* observation is marked with a vertical solid line. The orbital phase of the *NuStar* observation was about 0.65 (using the orbital parameters $P_{\rm orb}$=132.189 d and T_0=MJD 55425.6 Sugizaki et al. 2015). We have extracted data separately from both the modules using the standard *NuStar* data analysis software (NUSTARDAS V2.1.4) included in HEASOFT V6.34[a] along with the calibration database CALDB version 20240826. The NUPIPELINE task (version 0.4.12) was run with SAAMODE=strict and TENTACLE=yes because the background event rates were high to obtain clean event files.

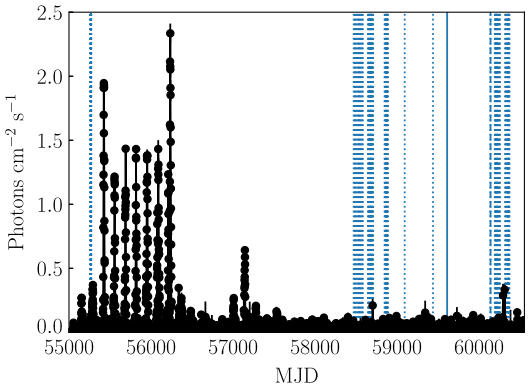

Figure 1. *MAXI* one day averaged light curve of GX 304-1 in the 2–20 keV energy band spanning the duration MJD 55054.5 (2009 August 11) until MJD 60545 (2024 August 23). The solid, dotted and dashed vertical lines indicate the epochs of *NuStar*, *Swift*, and *XMM-Newton* observations, respectively. A few epochs of *Swift* observations before 2009 August 11 are not shown here as they precede the time since the *MAXI* mission became operational.

The event files were barycentered using the FTOOLS task 'barycorr'. We used a circular region of radius 80″ centred on the source to extract the source events for both FPMA and FPMB modules. The NUPRODUCTS task was used to generate light curves binned in 1 s.

2.2 XMM-Newton observation

XMM-Newton (Jansen et al. 2001) observations of GX 304-1 were carried out on 2023 July 11 (MJD 60137, ObsID 0931790601) for a total duration of about 8 ks at an orbital phase of about 0.65 (using the orbital parameters $P_{\rm orb}$=132.189 d and T_0=MJD 55425.6 Sugizaki et al. 2015) which is similar to the orbital phase of the *NuStar* 2022 observation. *XMM-Newton* has three European Photon Imaging Camera (EPIC) cameras viz. one pn and two metal oxide semi-conductor (MOS) cameras (Strüder et al. 2001; Turner et al. 2001). The EPIC cameras were operated in the large window mode during this observation. The time resolution for the pn camera and the two MOS cameras used during this observation was 48 ms and 0.9 s, respectively. Observation Data Files (ODFs) were processed using version 21.0.0 of the *XMM-Newton* Science Analysis System (SAS)[b] and the current calibration files (CCF)[c] released on 2024 April 29. We searched for possible intervals of high instrumental background which yielded a negative result. The effective source exposures were about 5 and 7 ks for the pn and MOS cameras, respectively. We corrected the event arrival times to the solar system barycenter using SAS's 'barycen' task. A circular region of radius 30″ and 40″ was used to extract the source events for the pn and the MOS cameras. Background events were extracted using circular regions away from the source with radii of 70″, 60″, and 50″ for the pn, MOS1, and MOS2 cameras, respectively. We selected all the events in the energy range 0.3–10 keV, with pattern range 0–4 for the pn camera and 0–12 for the two MOS cameras. The averaged count rate for the pn and MOS cameras was about 1 and 0.4 counts s^{-1}, respectively. The

[a] https://heasarc.gsfc.nasa.gov/docs/software/lheasoft/.

[b] https://www.cosmos.esa.int/web/xmm-newton/sas.

[c] https://www.cosmos.esa.int/web/xmm-newton/current-calibration-files.

https://doi.org/10.1017/pasa.2025.12 Published online by Cambridge University Press

background contribution to the total count rate was negligible for EPIC cameras (averaged count rate of about 0.01 counts s^{-1}).

2.3 Swift observations

The *Neil Gehrels Swift Observatory* (Gehrels et al. 2004) observed GX 304-1 for various durations spanning the period from 2005 April 6 (MJD 53466) until 2024 February 27 (MJD 60367.8). *Swift* has three onboard instruments viz. the Burst Alert Telescope (BAT, Krimm et al. 2013), the X-Ray Telescope (XRT, Burrows et al. 2005), and the Ultraviolet/Optical Telescope (UVOT, Roming et al. 2005). We have used the data from only the XRT and the UVOT instruments in this work. The log of *Swift*/XRT observations used in this study before regular outbursts were detected from the pulsar around 2010 April is given in Table A1. The pulsar entered a low luminosity state around 2017 September and was found to be in the same state until around 2018 October (Escorial et al. 2018). We have analysed all available *Swift* observations since 2018 October to probe if the pulsar continues to remain in a similar low accretion regime, and these observations are listed in Table A2. *Swift*/XRT observations were mostly carried out in the photon counting (PC) mode having a time resolution of about 2.5 s. The *Swift*/XRT light curves for each epoch were extracted using the online tools (Evans et al. 2009)[d] hosted by the UK Swift Science Data Centre. The typical on-source effective exposures are about 1 ks for each *Swift*/XRT pointing.

Swift/UVOT archival observations of GX 304-1 are available from 2006 September 20 (MJD 53998.1) until 2024 February 27 (MJD 60367.8), having typical exposure times of about a few tens of seconds to a few hundreds of seconds at different epochs. UVOT observations were performed with the filters V ($\lambda = 546.8$ nm, $\delta\lambda = 76.9$ nm), B ($\lambda = 439.2$ nm, $\delta\lambda = 97.5$ nm), U ($\lambda = 346.5$ nm, $\delta\lambda = 78.5$ nm), UVW1 ($\lambda = 260.0$ nm, $\delta\lambda = 69.3$ nm), UVM2 ($\lambda = 224.6$ nm, $\delta\lambda = 49.8$ nm), and UVW2 ($\lambda = 192.8$ nm, $\delta\lambda = 65.7$ nm).[e] The Level2 UVOT data were analysed using the UVOTSOURCE tool from HEASOFT v6.34 to determine magnitudes and fluxes. A circular region of radius 5″ and 20″ were used to select the source region and background region, respectively. The source was detected in the UVOT filters V, B, U, UVW1, UVM2, and UVW2 having an averaged magnitude of about 14, 15.7, 16.6, 17.9, 20.9, and 19.2, respectively.

3. Analysis and results

3.1 Timing analysis

We used the *NuStar* combined FPMA and FPMB light curves in the 3–30 keV energy band for timing analysis. The FTOOLS[f] subroutine EFSEARCH was used to search for pulsations using the chi-squared maximisation method (Leahy et al. 1983). The inferred spin period from *NuStar* 2022 January (MJD 59608.5) observations is 275.425±0.003 s. The error on the measured spin period is estimated by fitting a Gaussian to the chi-square versus spin period plot obtained by EFSEARCH. The 1-σ error on the Gaussian centre estimate is taken as the error on the spin period. The estimated spin period is consistent with the known spin period of GX 304-1. The previous measured spin period of the source was about 275.12 s on 2018 June 3 (MJD 58272.25) (Escorial et al. 2018), which suggests that the source has spun down by about 0.3 s. The folded pulse profile in the 3–30 keV energy band using *NuStar* observations is shown in Fig. 2.

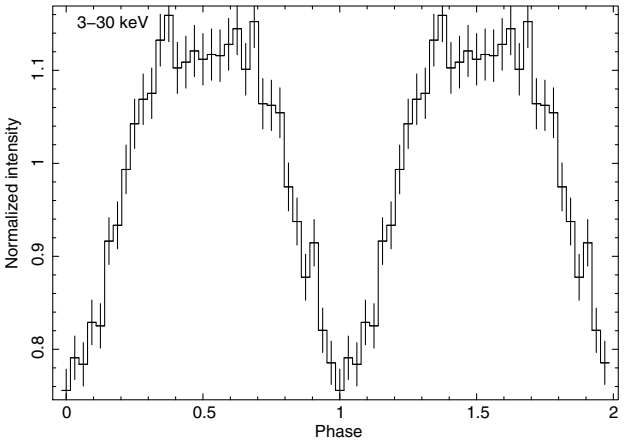

Figure 2. *NuStar* folded profile in the energy band of 3–30 keV obtained from the combined FPMA and FPMB light curve.

The estimated pulsed fraction ($PF = (I_{max} - I_{min})/(I_{max} + I_{min})$, where I_{max} and I_{min} are the maximum and minimum intensities in the folded profile, respectively) in the 3–30 keV energy band is about 21%. A similar folded pulse profile and PF in the 3–30 keV energy band was obtained from the *NuStar* observations of the pulsar carried on 2018 June 3 (Escorial et al. 2018) which suggests that the profile shape has not changed during this period. Similar PF of about 20% in the 3–20 keV energy band was obtained during the February-January 2012 INTEGRAL observations of the pulsar (Klochkov et al. 2012).

We have used the *XMM-Newton* pn data for timing analysis as the pulsar is relatively fainter in the MOS data. We used the pn 0.3–10 keV light curve binned in 10 s for timing analysis. The spin period estimated using EFSEARCH is 275.5±0.3 s. The error on the estimated spin period is obtained by the method described earlier. The folded profile in the 0.3–10 keV band using the pn light curve is shown in Fig. 3 which shows the presence of two peaks at low energies. Similar folded pulse profiles having two dominant peaks in soft X-rays (<10 keV) have been detected during outbursts of the pulsar in 2010 August (Devasia et al. 2011). The estimated PF from EPIC pn observations of the pulsar is about 25%.

3.2 Spectral analysis

The *NuStar* spectra were extracted from the same extraction parameters used for the light curves. We have done a combined fit of *NuStar*'s FPMA and FPMB data using XSPEC 12.14.1. The data have been binned using a minimum of 30 counts per bin. We have used a multiplicative model constant CONST to account for cross-instrument calibration uncertainties. The value of this constant was frozen at 1 for FPMA and was kept free for FPMB. The spectral fitting using XSPEC 12.14.1 (Arnaud 1996) was limited to 3–20 keV as the background dominates at higher energies. We fitted the combined spectra using an absorbed *PL+BB* model as shown in Fig. 4. We have used the *tbabs* model (Wilms, Allen, & McCray 2000) to take care of absorption in the spectrum during spectral fitting. As keeping the N_H free did not allow us to constrain the absorption, we kept it fixed at 9.6×10^{21} cm^{-2} which

[d] https://www.swift.ac.uk/user_objects/.
[e] https://www.mssl.ucl.ac.uk/www_astro/uvot/uvot_instrument/filterwheel/filterwheel.html.
[f] https://heasarc.gsfc.nasa.gov/ftools/ftools_menu.html.

https://doi.org/10.1017/pasa.2025.12 Published online by Cambridge University Press

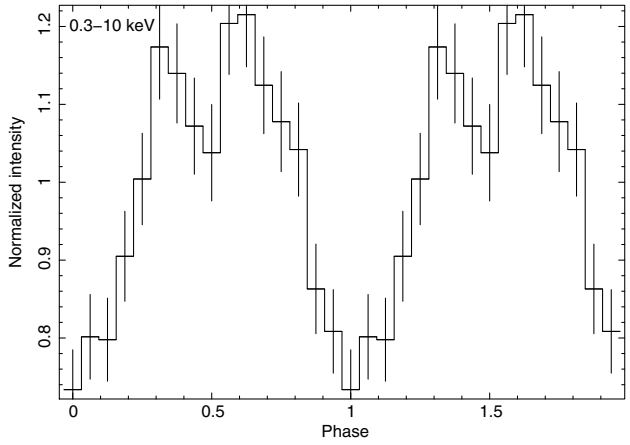

Figure 3. *XMM-Newton* folded profile of GX 304-1 in the energy band of 0.3–10 keV using data from EPIC pn observations.

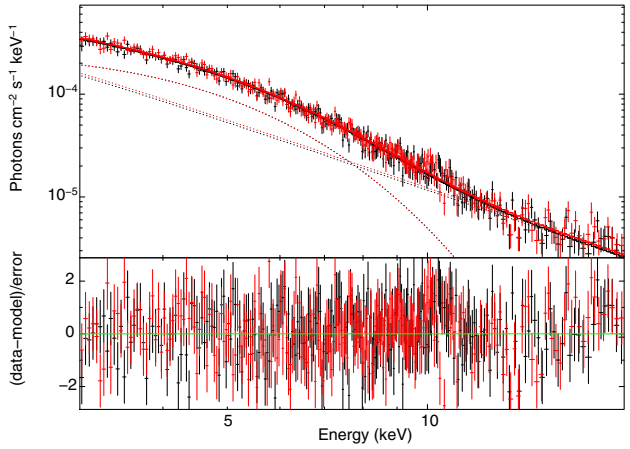

Figure 4. Spectrum of GX 304-1 obtained from *NuStar*'s FPMA (black) and FPMB (red), along with the best-fitting *PL+BB* model. The residuals between the data and the model are shown in the lower panel.

is the interstellar Galactic absorption along the direction of this source (HI4PI Collaboration et al. 2016).[g] The best-fit parameters obtained using this model were $\Gamma = 2.21^{+0.12}_{-0.14}$, $kT_{\rm BB} = 1.17^{+0.03}_{-0.02}$ keV, with χ^2_ν/d.o.f = 1.02/476. Using a source distance of 2.01 kpc, we obtained a *BB* radius $R_{\rm BB} = 100^{+7}_{-8}$ m. The unabsorbed flux in the energy range 3–20 keV is $\sim 7.5 \pm 0.1 \times 10^{-12}$ erg cm^{-2} s^{-1}, which implies a source luminosity of about 3.6×10^{33} erg s^{-1} for a distance of 2.01 kpc. The estimated luminosity in the 0.5–100 keV energy range is $\sim 1 \times 10^{34}$ erg s^{-1} using the WebPIMMS tool.[h]

The *XMM-Newton* spectra for the pn and MOS cameras were extracted using the same extraction parameters used to extract the source and background light curves. The response matrices and ancillary files were generated using the tasks `rmfgen` and `arfgen`. The pn and MOS spectra were rebinned with a minimum of 25 counts per bin to ensure the applicability of the χ^2 statistics. We have used XSPEC 12.14.1 (Arnaud 1996) for spectral fitting in the energy band of 0.5–10 keV. All spectral uncertainties are given at the 90% confidence level for each parameter. We checked that the separate fits of the pn and the MOS data gave similar results and then fitted them simultaneously to improve the statistics. The inter-calibration among the three instruments was accounted for using CONST.

We first fitted the spectra using an absorbed power-law (*PL*) model. We obtained hydrogen column density $N_{\rm H} = (2.36 \pm 0.14) \times 10^{22}$ cm^{-2} and a photon-index $\Gamma = 1.83 \pm 0.06$, with χ^2_ν/d.o.f. = 1.47/249. The fit using the absorbed-PL model was unacceptable and so we fitted the spectra using an absorbed blackbody (*BB*) model (Fig. 5(a)) which resulted in $N_{\rm H} = (7.14 \pm 0.06) \times 10^{21}$ cm^{-2}, a *BB* temperature $kT_{\rm BB} = 1.16 \pm 0.02$ keV, with χ^2_ν/d.o.f. = 1.12/245. It should be noted that the fitted $N_{\rm H}$ in this model is slightly less than the interstellar absorption ($N_{\rm H} \sim 9.6 \times 10^{21}$ cm^{-2}) along the direction of this source. Using a source distance of 2.01 kpc, we obtained a *BB* radius $R_{\rm BB} = 132 \pm 5$ m. The unabsorbed flux is $8.0 \pm 0.2 \times 10^{-12}$ erg cm^{-2} s^{-1} in the energy range of 0.5–10 keV, which implies a source luminosity of $3.9 \pm 0.1 \times 10^{33}$ erg s^{-1} for a distance of 2.01 kpc.

We also tried fitting the *PL+BB* model as shown in Fig. 5(b) and the best-fit parameters obtained using this model were $N_{\rm H} = (1.48^{+0.29}_{-0.31}) \times 10^{22}$ cm^{-2}, $\Gamma = 1.65^{+0.44}_{-0.43}$, $kT_{\rm BB} = 1.10^{+0.10}_{-0.09}$ keV, with χ^2_ν/d.o.f = 0.91/243. Using the F-test analysis, the probability that the improvement in the fit occurs by chance was found to be 1×10^{-24} and 1×10^{-11} in comparison with the single PL and BB models, respectively. Using a source distance of 2.01 kpc, we obtained a *BB* radius $R_{\rm BB} = 113^{+21}_{-15}$ m. The unabsorbed flux in the energy range 0.5–10 keV is $5.2 \pm 1.3 \times 10^{-12}$ erg cm^{-2} s^{-1}, which implies a source luminosity of about $2.5 \pm 0.6 \times 10^{33}$ erg s^{-1} for a distance of 2.01 kpc. The estimated luminosity in the 0.5–100 keV energy range is $\sim 7 \times 10^{33}$ erg s^{-1} using the WebPIMMS tool.

3.3 Long-term spin evolution in GX 304-1

We use all the spin period measurements reported in the literature, those measured by the *FERMI*/GBM observations and the spin periods estimated in this work from *NuStar* and *XMM-Newton* observations to construct the long-term spin history of GX 304-1, which is shown in Fig. 6. The spin evolution of this pulsar spans nearly five decades (February 1977 until July 2023). 272 s pulsations from the source were detected by McClintock et al. (1977) using *SAS-3* observations, which were also detected by Huckle et al. (1977) using *Ariel V* observations. Thereafter, the source became quiescent for almost three decades when it was detected using *INTEGRAL* observations (Manousakis et al. 2008). Pulsations having a periodicity of about 275.5 s was detected by *FERMI*/GBM during the onset of an outburst in 2010 April which suggests that the pulsar spun down by about 3.3 s during the long dormant period. The estimated spin-down rate during this quiescent period is $\sim -4.3 \times 10^{-14}$ Hz s^{-1} which is similar to those detected in other BeXRB pulsars during long (∼yr) dormant periods (Malacaria et al. 2020; Chandra, Roy, & Agrawal 2023). During the active period since 2010, the pulsar underwent a series of regular outbursts until 2013 before the outburst decayed. The pulsar exhibited spin-up during outbursts at a rate of $\sim 1 \times 10^{-12}$ Hz s^{-1} (Sugizaki et al. 2017; Malacaria et al. 2020) and spin-down between outbursts at a rate of $\sim -5 \times 10^{-14}$ Hz s^{-1} (Malacaria et al. 2020). The long-term spin-up rate during this active episode of the pulsar was estimated to be $\sim 1.3 \times 10^{-13}$ Hz s^{-1} (Malacaria et al. 2020).

The pulsar was detected by *FERMI*/GBM around MJD 57005 (2014 December 14) and MJD 57008 (2014 December 17) having spin period of about 274.8 s suggesting that the pulsar had undergone a change from a long-term spin-up to a spin-down trend

[g] https://heasarc.gsfc.nasa.gov/cgi-bin/Tools/w3nh/w3nh.pl.
[h] https://heasarc.gsfc.nasa.gov/cgi-bin/Tools/w3pimms/w3pimms.pl.

https://doi.org/10.1017/pasa.2025.12 Published online by Cambridge University Press

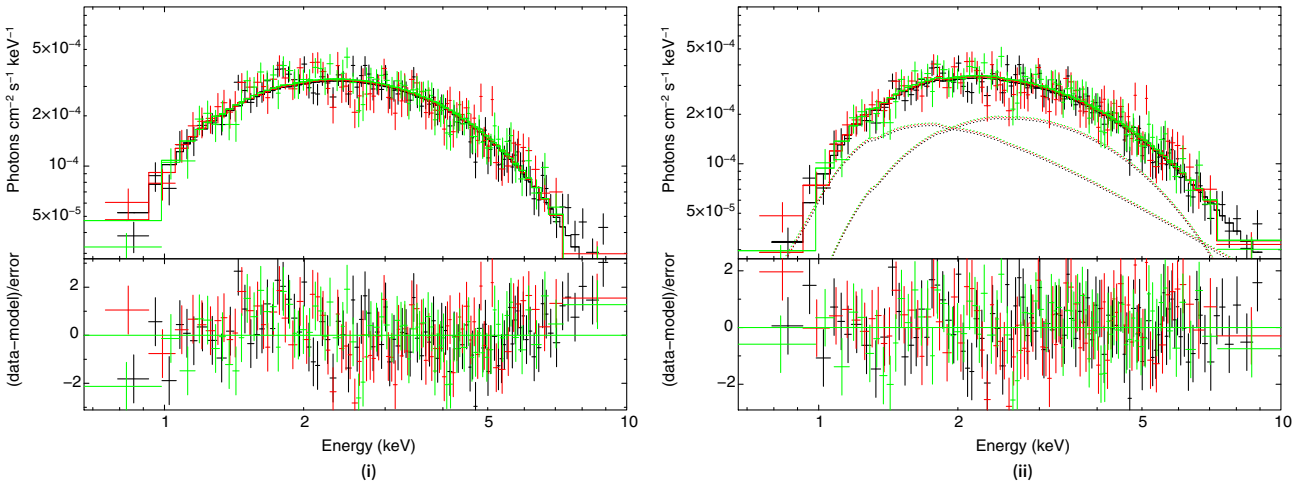

Figure 5. (a) Spectrum of GX 304-1 fitted with the absorbed blackbody model. The spectra of the pn, MOS1, and MOS2 cameras are shown in black, red, and green, respectively. The residuals between the data and the model are shown in the lower panel. (b) The same spectra shown in (a) fitted with the absorbed powerlaw+blackbody model with the residuals between the data and the model shown in the lower panel.

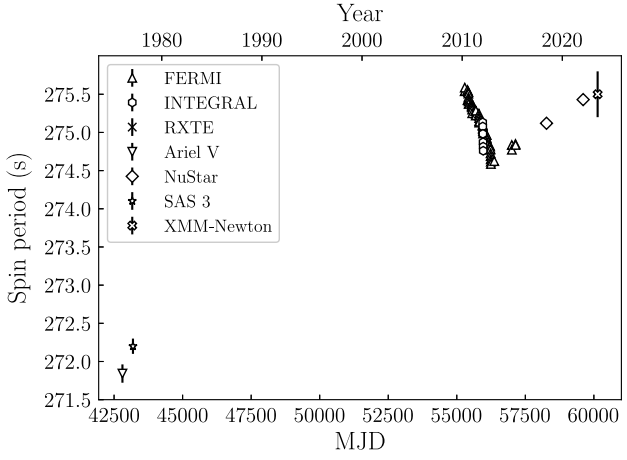

Figure 6. Long-term spin history of GX 304-1 from 1977 February until 2023 July. The reversal in trend from long-term spin-up to long-term spin-down of the X-ray pulsar is discernible between the period 2010–2023.

during the preceding quiescent episode of the pulsar. Interestingly, the pulsar was again detected after one orbital period (about 132 d) around MJD 57140 (2015 April 28) and MJD 57143 (2015 May 1) having a similar spin period of about 274.8 s which confirms the onset of spin-down episode of the pulsar. The spin period measured using *NuStar* observation during the low X-ray luminosity state of the pulsar around MJD 58272 (2018 June 3) was 275.12±0.02 s (Escorial et al. 2018). Spin periods estimated in this work using the *NuStar* and the *XMM-Newton* observations from 2022 January and 2023 July corroborates the detection of a long-term spin-down manifestation in this pulsar. The estimated long-term spin-down rate is $\sim -3.4 \times 10^{-14}$ Hz s^{-1} which is similar to those detected during spin-down periods between X-ray outbursts in this source. This suggests that the underlying mechanism of spin-down between regular outbursts observed in this source during 2010–2013 and that during the ongoing quiescent period since 2015 might be the same. Spin variations on long time-scales have been detected in several accretion-powered pulsars (Makishima et al. 1988; Nagase 1989; Bildsten et al. 1997; Chakrabarty et al. 1997; Fritz et al. 2006; Camero-Arranz et al. 2009; Inam, Şahiner, & Baykal 2009; González-Galán et al. 2012; Chandra et al. 2021).

3.4 X-ray activity during change in long-term spin trend

The X-ray light curves in the 2–20 keV and 15–50 keV energy bands from the *MAXI* and *Swift*/BAT monitoring observations of the source are shown in Fig. 7. The light curves are plotted for the period spanning MJD 56380-57000 (2013 March 29–2014 December 9) when the source underwent spin evolution from a long-term spin-up to spin-down trend and was undetected by *FERMI*/GBM observations. The dotted vertical lines in the figures show the epochs of periastron passages using the orbital parameters $P_{\rm orb}$=132.189 d and T_0=MJD 55425.6 (Sugizaki et al. 2015). There is an indication of a weak X-ray brightening of the source during periastron passages around MJD 56482 (2013 July 9), MJD 56614 (2013 November 18), MJD 56746 (2014 March 30), and MJD 56879 (2014 August 10) which is seen in both *MAXI* and *Swift*/BAT observations. The estimated X-ray luminosities during these periastron passages are about 2×10^{35}, 7×10^{34}, 6×10^{34}, and 2×10^{34} erg s^{-1} which suggests that accretion is not quenched during this period. The luminosities are inferred using the luminosities given in Tsygankov et al. (2019) when the source was in a low luminosity state and then scaling the luminosity using the *MAXI* count rate for a given epoch (assuming that there is no spectral evolution at low luminosities which is confirmed by Escorial et al. 2018).

3.5 Long term photometric observations of the companion star

The long-term photometric observations of the companion star V850 Cen is shown in Fig. 8. We have plotted the V-band magnitudes reported in the literature (Corbet et al. 1986; Haefner 1988) during the period MJD 44285.5 (1980 February 16) until MJD 46121.5 (1985 February 25) along with those obtained from the

https://doi.org/10.1017/pasa.2025.12 Published online by Cambridge University Press

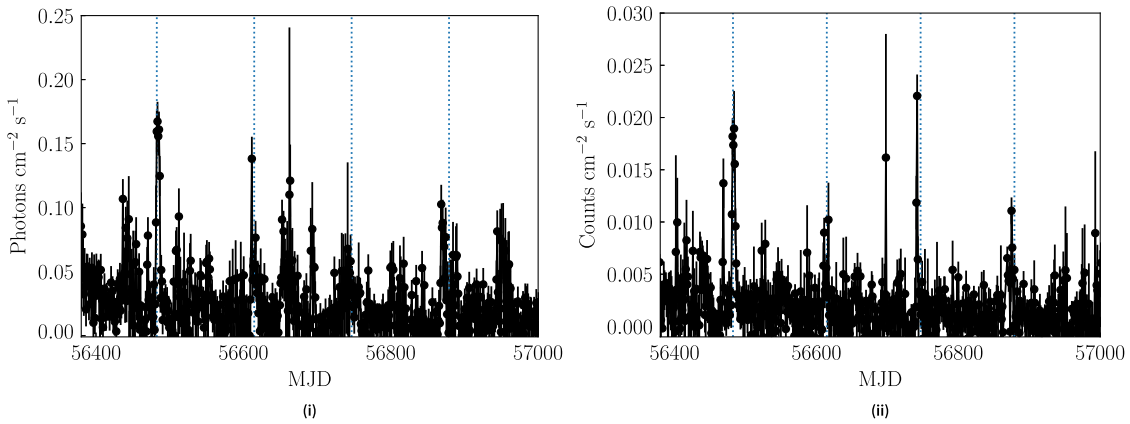

Figure 7. (a) *MAXI* one day averaged light curve of GX 304-1 in the 2–20 keV energy band spanning the duration when the change in long-term spin trend occurred in this pulsar. The dotted vertical lines indicate the epochs of periastron passages of the neutron star. (b) *Swift*/BAT one day averaged light curve of GX 304-1 in the 15–50 keV energy band shown during the same duration with times of periastron passages marked with vertical dotted lines.

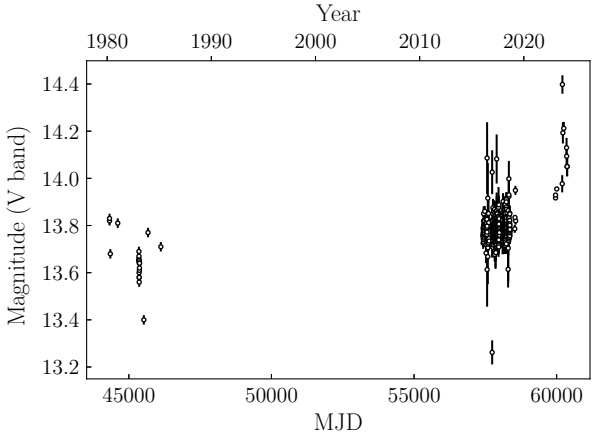

Figure 8. Long-term photometric observations of the companion star of GX 304-1 using observations reported in the literature (Corbet et al. 1986; Haefner 1988) spanning the duration MJD 44285.5 until MJD 46121.5 and those obtained from the ASAS-SN optical observations (https://asas-sn.osu.edu/), AAVSO (https://www.aavso.org/) and *Swift*/UVOT.

ASAS-SN optical observations (https://asas-sn.osu.edu/), AAVSO (https://www.aavso.org/), and *Swift*/UVOT. The averaged V-band magnitude during the period spanning almost five years from 1980–1985 was ∼13.6, while that during the period MJD 57423.7 (2016 February 5) to MJD 60367.8 (2024 February 27) was ∼13.9. Optical brightening of the companion star in BeXRBs has been associated with X-ray outbursts in these systems (Corbet et al. 1985; Negueruela et al. 1997; Reig et al. 2007; Caballero-Garca et al. 2016; Coe et al. 2024).

The increase in averaged V-band magnitude by about 0.3 suggests that the companion star has become relatively less active recently due to which there have likely been no episodes of mass ejection from the companion star that feeds the relatively bright X-ray outbursts in this binary pulsar. This is confirmed by the weak X-ray detection of the pulsar on MJD 57411 (2016 January 24) and MJD 57525 (2016 May 17) at a flux level of 23±4 mCrab and 22±14 mCrab respectively using *MAXI* observations (Nakajima et al. 2016b,a) after which the pulsar has remained dormant. Unfortunately, no regular optical monitoring observations of the source is available during the period when the pulsar switched from a long-term spin-up trend to spin-down except for one optical spectroscopic observation (around MJD 56763 (2014 April 16)) using the the 3.9 m *Anglo Australian Telescope* (*AAT*) which suggested that the radius of the decretion disc around the companion star had shrunk significantly (by almost a factor of 2) compared to the epochs when the pulsar was moderately active in X-rays (Malacaria et al. 2017).

3.6 Long-term ultraviolet observations of the companion star

The X-ray (2–20 keV) and ultraviolet light curves for GX 304-1 obtained from *MAXI* and *Swift*/UVOT observations are shown in Fig. 9. The *Swift*/UVOT light curves show the inferred fluxes in the U, UVW1, and the UVW2 filters. The ultraviolet fluxes of the source show a marked gradual increase around MJD 55300 (2010 April) until around MJD 56000 (2012 March) in all three filters (U, UVW1, and UVW2) which interestingly coincides with the re-kindling of the X-ray outbursts detected in this pulsar as observed from simultaneous *MAXI* X-ray light curve. The increase in the ultraviolet fluxes in the U, UVW1 and the UVW2 filters are about a factor of 2.3, 2, and 1.5 during the dormant period (around MJD 55268) compared to that during the beginning of X-ray outbursts (around MJD 55550). It also seems that the increase in the ultraviolet activity of the companion star preceded the onset of bright X-ray outbursts by about half a year. A similar increase in the ultraviolet flux in the UVW1 band preceded the onset of X-ray outbursts in the BeXRB Swift J004516.6-734703 by about a year (Kennea et al. 2020). The increase in UV flux was attributed to the formation of a circumstellar disc around the companion star in Swift J004516.6-734703 (Kennea et al. 2020). It is likely that the increase in the UV signatures in GX 304-1 might also indicate the resurgence of the formation of a decretion disc around the companion star which was big enough to trigger bright X-ray outbursts in the binary after about half a year. After the regular X-ray outbursts ceased in GX 304-1, the ultraviolet fluxes in the three bands have shown little long-term variation with no indication of returning to the pre-outburst level. However, there is suggestion of a decrease in the ultraviolet fluxes around MJD 60300 (2023 December) on short timescales.

https://doi.org/10.1017/pasa.2025.12 Published online by Cambridge University Press

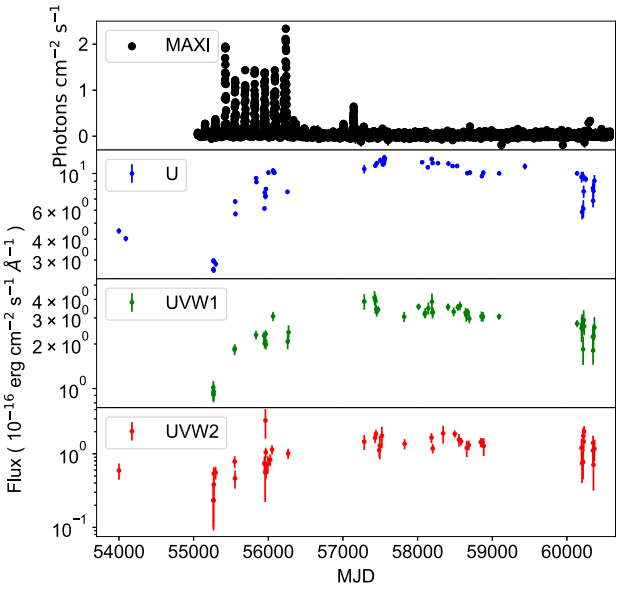

Figure 9. Long-term X-ray and ultraviolet observations of GX 304-1 as observed with *MAXI* and *Swift*/UVOT, respectively. We show, from top to bottom, the one-day averaged X-ray count rate in the 2–20 keV band from *MAXI* and the UV fluxes in the U, UVW1, and UVW2 bands from *Swift*/UVOT.

3.7 Long-term quiescent X-ray activity of GX 304-1 using Swift/XRT

The long-term *Swift*/XRT light curve of GX 304-1 in the 0.3–10 keV band is shown in Fig. 10(a) for the duration spanning 2005 April 6 (MJD 53466) until 2010 March 15 (MJD 55270.86) and in Fig. 10(b) for the period from 2018 December 17 (MJD 58469) until 2024 February 27 (MJD 60367.8). The count rates have been averaged for a given epoch. It is observed that the XRT count rate during the period between MJD 53466-55270.86 varied from about ∼0.4 counts s^{-1} to ∼1.2 counts s^{-1} showing a dynamic range of about 3. The averaged count rate during this period was about 0.7 counts s^{-1}. This suggests that the pulsar was moderately active in X-rays but did not undergo an outburst as the peak XRT count rates even during weak outbursts in 2016 February was about 2–4 counts s^{-1} (Escorial et al. 2018).

The XRT count rate spanning the duration 2018 December 17 until 2024 February 27 varied from about 0.06–0.3 counts s^{-1} (having a dynamic range of about 5) which suggests that the pulsar was in a low X-ray activity state. This quiescent behaviour of the pulsar is similar to that observed from 2016 June until 2018 October when the XRT count rate varied in the range of about 0.1–0.25 counts s^{-1} (Escorial et al. 2018). The averaged count rate during this period was about 0.2 counts s^{-1}. As seen in Fig. 10(b), the pulsar also did not exhibit any clear enhancement in X-ray activity at periastron passages. This intriguing low luminosity state of the source has now lasted for about seven years since September 2017. Similar long-term quiescent episodes on nearly decadal timescales has been detected in other Be/X-ray binaries such as 1A 0535+262, GS 0834-430, RX J0209.6-7427, XTE J1946+274, 2S 1417-624, KS 1947+300, and RX J0440.9+4431 (Usui et al. 2012; Miyasaka et al. 2013; Gupta, Naik, & Jaisawal 2019; Chandra et al. 2020, 2023; Liu et al. 2023).

4. Discussions

In the following section, we discuss plausible mechanisms that can lead to a long-term spin-down and low luminosity state in this pulsar.

4.1 Quasi-spherical accretion in GX 304-1

The long-term spin-down in this pulsar can be explained using the theory of quasi-spherical accretion from the stellar wind of the companion star (Shakura et al. 2012; Shakura et al. 2014). The conditions for the applicability of this model such as slow spin period and X-ray luminosity $< 4 \times 10^{36}$ erg s^{-1} are fulfilled by GX 304-1 observations. The spin period of this pulsar is about 275 s and the inferred X-ray luminosity during the period when the spin evolution changed from a long-term spin-up to the spin-down regime is about 2×10^{35} erg s^{-1} except during bright outbursts of the source when the luminosity reaches about 10^{37} erg s^{-1} (Yamamoto et al. 2011a; Klochkov et al. 2012; Malacaria et al. 2015; Sugizaki et al. 2015; Jaisawal, Naik, & Epili 2016). The inferred luminosity during the low state of the pulsar from *XMM-Newton* observations (when the pulsar was spinning down) is about 2.5×10^{33} erg s^{-1} in the 0.5–10 keV energy band. The spin-up during outbursts and spin-down on short time-scales in between regular outbursts have been explained using this model by Postnov et al. (2015). Using the quasi-settling accretion theory, the estimated spin-down rate is given by Postnov et al. (2015),

$$\dot{\omega}^*_{sd} \sim 10^{-8} \frac{Hz}{d} \Pi_{sd} \mu_{30}^{13/11} \dot{M}_{16}^{3/11} \left(\frac{P^*}{100\ \mathrm{s}} \right)^{-1}, \qquad (1)$$

where $\mu_{30} = \mu/10^{30}$[G cm^3] is the dipole magnetic moment given by $\mu = \mathrm{BR}^3/2$ where R is the radius of the neutron star having a typical value of 10 km, $\dot{M}_{16} = \dot{M}/10^{16}$[g s^{-1}] is the mass accretion rate onto the neutron star and P^* is the equilibrium spin period of the neutron star. We obtain $\dot{\omega}^*_{sd} \sim -3.1 \times 10^{-8}$ Hz/d (using $\Pi_{sd} \sim 4.6$ (Shakura et al. 2012; 2014; Postnov et al. 2015), $\dot{M}_{16} = 0.22$ using $\mathrm{L_X} = 0.1\dot{M}c^2$ and $\mathrm{L_X} = 2 \times 10^{35}$ erg s^{-1}, $\mu_{30} = 2.35$ and $P^*_{eq} = 275$ s) which is slightly larger than the estimated long-term spin-down rate by a factor of ∼1.7. Fig. 11 shows the observed spin-up/down rates obtained from a linear fit of spin evolution of the pulsar during spin-up/down episodes.

The spin-up rate estimated during outbursts using the quasi-settling accretion theory is $\sim 2.5 \times 10^{-7}$ Hz/d (Postnov et al. 2015). The dotted horizontal lines in Fig. 11 show the estimated spin-up/spin-down rates using the quasi-spherical settling accretion theory. The long-term spin-down rates are remarkably similar to the short time-scale spin-down rates estimated between outbursts in this source which suggests that both the short-term and long-term spin-down might be caused by the same mechanism in this pulsar. The long-term spin-up rate is about a factor of 4 smaller than the spin-up rates estimated during X-ray outbursts detected in this pulsar. Thus, this model can estimate the spin-down rate within a factor of ∼1.7 and may qualitatively explain the long-term spin-down in this pulsar. Quasi-spherical accretion has been used to explain the long-term spin-down episodes in GX 1+4 and Vela X-1 (Shakura et al. 2012; Chandra et al. 2021).

4.2 Tug of war between spin-up and spin-down torques

It is observed around MJD 56000 (ref. Fig. 11) that the spin-up rates estimated during outbursts seem to diminish systematically with time (except for one instance of rapid spin-up during a giant

https://doi.org/10.1017/pasa.2025.12 Published online by Cambridge University Press

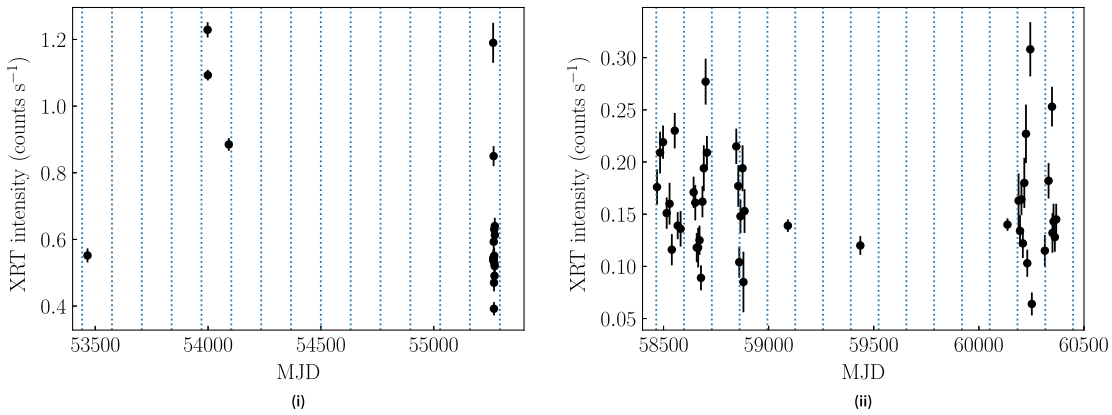

Figure 10. (a) *Swift*/XRT light curve (0.3–10 keV energy band) of GX 304-1 spanning the quiescent phase for the duration 2005 April 6 (MJD 53466) until 2010 March 15 (MJD 55270.86). The vertical dotted lines indicate the epochs of periastron passages of the neutron star. The averaged XRT count rate during this duration is about 0.7 counts s^{-1}. (b) Same as (a) for the duration spanning nearly five years from 2018 December 17 (MJD 58469) until 2024 February 27 (MJD 60367.8). The averaged XRT count rate during this duration is about 0.2 counts s^{-1}.

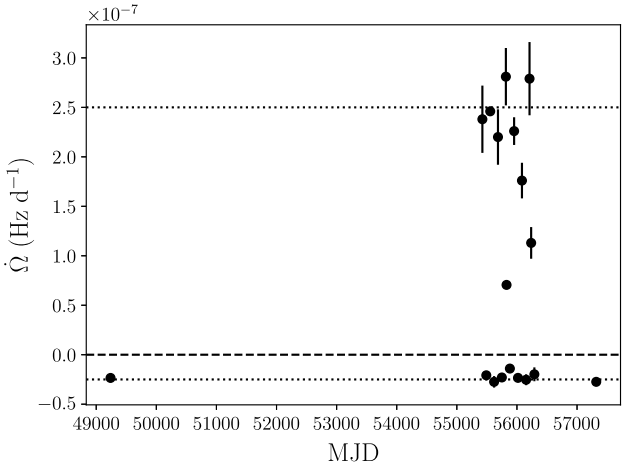

Figure 11. Plot showing estimated spin-up and spin-down rates spanning the duration of about five decades. The estimated spin-up and spin-down rates using the quasi-spherical settling accretion theory are shown using horizontal dotted lines (Shakura et al. 2012; Shakura et al. 2014; Postnov et al. 2015).

outburst detected in this pulsar) by a factor of about 2 as the pulsar changes trend from a long-term spin-up to spin-down. However, the spin-down rates inferred in between the outbursts remain nearly the same during this period (Fig. 11). The estimated peak X-ray flux in the 2–10 keV energy band during the spin-down episodes in between the outbursts diminished by a factor of about 1 000 compared to the flux during the spin-up regimes (ref. Table 1 in Postnov et al. 2015) which suggests that the accretion rate onto the neutron star ($\dot{M}$) decreased by the same factor during spin-down phases. The spin-up torque ($K_{\rm su}$) acting on the neutron star is given by Pringle & Rees (1972),

$$K_{\rm su} = \dot{M}(GM_{\rm ns}r_{\rm m})^{1/2}, \tag{2}$$

where G is the gravitational constant, $M_{\rm ns}$ is the mass of the neutron star and $r_{\rm m}$ is the radius at which the effective pressure in the accretion disc equals the magnetic pressure. As the accretion rate drops during the spin-down regimes, consequently the spin-up torque also decreases significantly during this period. The spin evolution of an accretion-powered pulsar is given by,

$$2\pi I\dot{\nu} = K_{\rm su} - K_{\rm sd}, \tag{3}$$

where I is the moment of inertia of the neutron star and $K_{\rm sd}$ is the spin-down torque acting on the neutron star. Assuming that the spin-down torque acting on the neutron star is nearly constant (which is observed in Fig. 11 that the estimated spin-down torques in between outbursts are almost the same), the spin-down torque would eventually overtake the decreasing spin-up torque (after around MJD 56200) leading to a long-term spin-down in the pulsar.

The estimated averaged X-ray luminosities (in the 0.5-100 keV energy range using the method described earlier) during the period MJD 57005-57008 and MJD 57140-57143 when the pulsar was already spinning down was $\sim 4.4 \times 10^{35}$ and $\sim 9.6 \times 10^{35}$ erg s^{-1}, respectively. These luminosities are about a factor of 10–100 smaller than those detected during bright X-ray outbursts in this pulsar which suggests that the increase in accretion rate during this period did not lead to a sufficient increase in the spin-up torque to change the long-term spin-down trend of the pulsar. The estimated luminosities after about a year around MJD 57423 and MJD 57506 were about 1.2×10^{35} and 2.8×10^{34} erg s^{-1}, respectively (Rouco Escorial & Wijnands 2016). From long-term X-ray monitoring observations of the source spanning the duration around MJD 58000-58420, the estimated luminosities were found to lie in the range $\sim 0.8 - 1.9 \times 10^{34}$ erg s^{-1} (Rouco Escorial & Wijnands 2016). Recent *Swift*/XRT, *XMM-Newton* and *NuStar* observations analysed in this work confirm the prolonged low state of the pulsar. The relatively low luminosity of the pulsar since the last bright outburst detected in 2013 suggests relatively weak spin-up torque acting on the pulsar and the continued dominance of the spin-down torque over the spin-up torque. The estimated spin period of the source (275.12±0.02 s) around MJD 58272 (Rouco Escorial & Wijnands 2016) and those obtained from *NuStar* and the *XMM-Newton* observations in this work confirms this proposition as the pulsar continues to spin-down on long time-scales.

The long-term spin-down of the pulsar ($\sim -4.3 \times 10^{-14}$ Hz s^{-1}) changed to a short-term spin-up trend after the onset of outbursts in 2010 ($\sim 1.3 \times 10^{-13}$ Hz s^{-1}) with the averaged spin-up

https://doi.org/10.1017/pasa.2025.12 Published online by Cambridge University Press

rate being an order of magnitude higher than the long-term spin-down rate. This suggests that the average momentum imparted by the accreted material during the spin-up phase was greater than the momentum lost due to magnetic breaking over the long-term spin-down phase lasting about 28 yr which is also observed in SMC X-3 (Townsend et al. 2017). We now discuss possible mechanisms to explain the enigmatic long-term low luminosity state of the pulsar since 2018 December.

4.3 Propeller effect

The XRT count rates shown in Fig. 10 are converted into the corresponding 0.5–100 keV luminosities (Fig. 12) using the spectral study and luminosities from Tsygankov et al. (2019) (when the source was faint having an XRT count rate of about 0.13 counts s^{-1}) and then scaling our observed XRT count rates which are listed in Tables A1 and A2. An assumption is made during this conversion that the spectrum of the pulsar does not change during faint state which is confirmed by Escorial et al. (2018). The estimated luminosities shown in Fig. 12(a) for the duration 2005 April 6 (MJD 53466) until 2010 March 15 (MJD 55270.9) varied in the range of $\sim 3.7 - 11.2 \times 10^{34}$ erg s^{-1} showing variation by a factor of about 3. The luminosities for the duration spanning 2018 December 17 (MJD 58469) until 2024 February 27 (MJD 60367.8) is shown in Fig. 12(b) showing luminosities in the range of $\sim 0.6 - 2.9 \times 10^{34}$ erg s^{-1}, which suggests that the source has been quasi-stable in a low luminosity state for the last five years. The pulsar was in a slightly higher low luminosity regime during 2005 April 6–2010 March 15. Accreting pulsars may switch to the propeller regime at low mass accretion rates caused by the centrifugal barrier if the velocity of the rotating magnetosphere exceeds the local Keplerian velocity (Illarionov & Sunyaev 1975). The critical luminosity for the onset of the propeller effect ($L_{\rm prop}$) is given by Tsygankov et al. (2017),

$$L_{\rm prop} \simeq \frac{GM\dot{M}_{\rm prop}}{R} \simeq 4 \times 10^{37} k^{7/2} B_{12}^2 P_s^{-7/3} M_{1.4}^{-2/3} R_6^5 \ {\rm erg\ s^{-1}}, \quad (4)$$

where M, R, P_s and B are the mass, radius, spin period, and magnetic field of the neutron star, respectively. $\dot{M}_{\rm prop}$ is the mass-accretion rate onto the neutron star. The factor k is the ratio of the magnetospheric radius and the Alfvén radius which in the case of disc accretion is taken to be $k = 0.5$ (Ghosh & Lamb 1978). Using $M = 1.4\ {\rm M}_\odot$, R=10 km, $P_s \sim 275.4$ s, $B = 4.7 \times 10^{12}$ G (Yamamoto et al. 2011a) and $k = 0.5$ (assuming disc accretion), the estimated $L_{\rm prop}$ is $\sim 3.2 \times 10^{32}$ erg s^{-1} which is shown by a dashed horizontal line in Fig. 12(a) and (b).

The magnetic field ($B = 4.7 \times 10^{12}$ G Yamamoto et al. 2011a) used in estimating the limiting luminosity due to the onset of the propeller effect using equation (4) was obtained from the detection of cyclotron resonance scattering feature (CRSF) in the spectra. The magnetic field can also be estimated independently by using (Christodoulou, Kazanas, & Laycock 2016),

$$B = \left(2\pi^2 \xi^7\right)^{-1/4} \sqrt{\frac{GMI}{R^6} |\dot{P}_S|}\,, \quad (5)$$

where ξ is a dimensionless parameter which is the ratio of the inner edge of the accretion disc and the magnetospheric radius (Ghosh & Lamb 1979; Wang 1996; Christodoulou et al. 2016), M and R are the mass and the radius of the neutron star, respectively, I is the moment of inertia of the neutron star given by $I = \frac{2MR^2}{5}$ and $\dot{P}_S$ is the rate of spin change of the pulsar during outbursts. Using ξ=1, $M = 1.4\ {\rm M}_\odot$, $R = 10$ km, $\dot{P}_S \sim 3.1 \times 10^{-8}$ s s^{-1} (Postnov et al. 2015) and $G = 6.67 \times 10^{-8}$ cm^3 g^{-1} s^{-2}, the estimated magnetic field of the neutron star is $\sim 3.8 \times 10^{13}$ G, which is higher by a factor of about 8 than that inferred from the detection of cyclotron line in the spectra. Using $B \sim 3.8 \times 10^{13}$ G, the estimated luminosity for the onset of the propeller effect is $\sim 2.6 \times 10^{33}$ erg s^{-1}, which is about an order of magnitude higher than that estimated earlier. The magnetic field of the neutron star can also be estimated independently using the models given by Ghosh & Lamb (1979) and Kluźniak & Rappaport (2007), which are applicable to disc-fed systems. The Ghosh and Lamb model (Ghosh & Lamb 1979) is applicable to systems irrespective of whether they have achieved spin equilibrium and the model predicts (Klus et al. 2014)

$$-\dot{P} = 5.0 \times 10^{-5} \mu_{30}^{2/7} n(\omega_s) R_6^{6/7} \left(\frac{M}{M_\odot}\right)^{-3/7} I_{45}^{-1} (P L_{37}^{3/7})^2, \quad (6)$$

where $\dot{P}$ is the long-term spin derivative of the neutron star (in s yr^{-1}), I is the moment of inertia of the neutron star and $n(\omega_s)$ is the dimensionless accretion torque and depends on the fastness parameter ω_s (Ghosh & Lamb 1979; Klus et al. 2014). Using $\dot{P} \sim 0.08$ s yr^{-1}, $n(\omega_s) \sim 1$, $R = 10^6$ cm, $M = 1.4\ {\rm M}_\odot$, I_{45}=1.92 g cm^3, $P = 275$ s and $L \sim 2 \times 10^{37}$ erg s^{-1}, the magnetic field is estimated to be $\sim 5.5 \times 10^6$ G, which is lower by a factor of about 10^6 than that inferred from the detection of cyclotron line in the spectra. Using the Kluzniak and Rappaport model (Kluźniak & Rappaport 2007)

$$-\dot{P} = 8.2 \times 10^{-5} \mu_{30}^{2/7} g(\omega_s) R_6^{6/7} \left(\frac{M}{M_\odot}\right)^{-3/7} I_{45}^{-1} (P L_{37}^{3/7})^2, \quad (7)$$

where $g(\omega_s)$ depends on the fastness parameter ω_s and is nearly equal to unity. Using $\dot{P} \sim 0.08$ s yr^{-1}, $g(\omega_s) \sim 1$, $R = 10^6$ cm, $M = 1.4\ {\rm M}_\odot$, I_{45}=1.92 g cm^3, $P = 275$ s and $L \sim 2 \times 10^{37}$ erg s^{-1}, the magnetic field estimated using this model is $\sim 9.8 \times 10^5$ G, which is similar to that estimated using the Ghosh and Lamb model by within a factor of about 6. Similar lower magnetic field estimates compared to that inferred from cyclotron lines were obtained for accreting pulsars (not near spin equilibrium) by Klus et al. (2014) using the Ghosh and Lamb model (Ghosh & Lamb 1979) as well as the Kluzniak and Rappaport model (Kluźniak & Rappaport 2007). The magnetic field estimates obtained using the Ghosh and Lamb model and the Kluzniak and Rappaport model would reduce the threshold luminosity for the onset of the propeller effect by a factor of about 10^6 compared to that obtained using the magnetic field estimated using the cyclotron line.

The estimated luminosities of the pulsar during the faint state (Fig. 12) are well above the threshold luminosity (at least by a factor of about 19 for $L_{\rm prop} \sim 3.2 \times 10^{32}$ erg s^{-1} and by a factor of about 3 for $L_{\rm prop} \sim 2.6 \times 10^{33}$ erg s^{-1}) for the propeller effect to set in. Another telltale manifestation of the onset of the propeller effect is the sudden decrease in the luminosity of the pulsar as observed in 4U 0115+63 and V0332+53 (Campana et al. 2001; Tsygankov et al. 2016) which is not observed in GX 304-1. In addition, the detection of pulsations from the source using *NuStar* and *XMM-Newton* observations indicates that accretion is still continuing at low luminosities. Hence, the long-term low luminosity regime of the pulsar cannot be explained using the propeller effect.

https://doi.org/10.1017/pasa.2025.12 Published online by Cambridge University Press

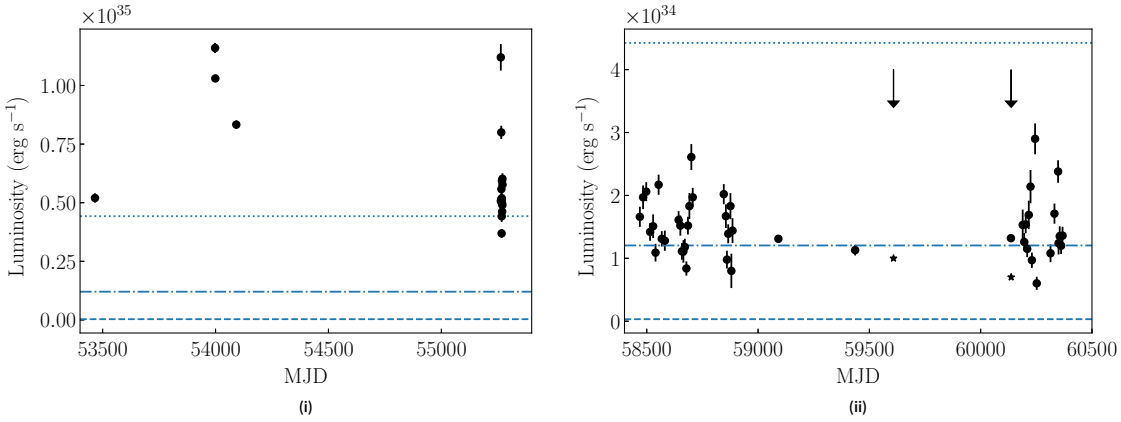

Figure 12. (a) Plot showing estimated X-ray luminosity (0.5–100 keV) of GX 304-1 spanning the duration 2005 April 6 (MJD 53466) until 2010 March 15 (MJD 55270.9). The horizontal dashed line shows the estimated limiting luminosity for the propeller effect to set in. The dotted and dash-dotted horizontal lines show the limiting luminosity for accretion to occur from a cold disc. The averaged X-ray luminosity (0.5–100 keV) during this duration is about 6.3×10^{34} erg s^{-1}. (b) Same as (a) for the duration spanning from 2018 December 17 (MJD 58469) until 2024 February 27 (MJD 60367.8). The averaged X-ray luminosity (0.5–100 keV) during this duration is about 1.5×10^{34} erg s^{-1}. The downward arrows show the epoch of the *NuStar* and the *XMM-Newton* observations used in this study and the estimated 0.5–100 keV unabsorbed luminosities for these epochs are shown by stars.

4.4 Sustained accretion from a cold disc?

The observed long-term low luminosity regime of the pulsar may be explained using accretion from a 'cold disc' wherein for low accretion rates well above the propeller regime, the temperature of the disc may fall below the Hydrogen ionisation temperature of about 6 500 K (Tsygankov et al. 2017). In this case, the matter in the disc is non-ionised (referred to as 'cold disc') and accretion can proceed through the cold disc (Tsygankov et al. 2017). Two criteria need to be satisfied for accretion from the cold disc. First, the accretion rate has to be sufficiently high to overcome the centrifugal barrier which implies that the luminosity of the source should be higher than the threshold luminosity for the propeller effect to take over which is satisfied during the *Swift*/XRT, *NuStar*, and *XMM-Newton* observations of GX 304-1 (ref. Fig. 12). Secondly, the luminosity of the source should be lower than the luminosity for stable accretion from a cold disc ($L_{\rm cold}$) given by Tsygankov et al. (2017),

$$L_{\rm cold} = 9 \times 10^{33}\, k^{1.5}\, M_{1.4}^{0.28}\, R_6^{1.57}\, B_{12}^{0.86} \quad {\rm erg\ s^{-1}}. \tag{8}$$

The above threshold for $L_{\rm cold}$ assumes that the disc temperature is highest at the magnetospheric radius and as a result the disc temperature for any radius lesser than the magnetospheric radius is less than 6 500 K (Tsygankov et al. 2017). Using $M = 1.4$ M$_\odot$, $R = 10$ km, $B = 4.7 \times 10^{12}$ G (Yamamoto et al. 2011a) and $k = 0.5$ (assuming disc accretion), the estimated $L_{\rm cold}$ is $\sim 1.2 \times 10^{34}$ erg s^{-1} which is shown by a dash-dotted horizontal line in Fig. 12(a) and (b).

The observed 0.5–100 keV luminosities of the source lies within a factor of about 2–3 times the $L_{\rm cold}$ estimated for the source during the period since December 2018 and within a factor of about 3–10 during the period spanning 2005 April 6 (MJD 53466) until 2010 March 15 (MJD 55270.9). It should be noted that the equation (8) does not take into account the interaction between the pulsar magnetosphere and the accretion disc and a more accurate threshold for $L_{\rm cold,acc}$ is given by Tsygankov et al. (2017),

$$L_{\rm cold,acc} \simeq 7 \times 10^{33}\, A^{-7/13}\, k^{21/13}\, M_{1.4}^{3/13}\, R_6^{23/13} B_{12}^{12/13}\, T_{6500}^{28/13} \ {\rm erg\ s^{-1}}, \tag{9}$$

where A is given by,

$$A = \begin{cases} 0.057\, \beta^{-6}, & \text{if} \quad \beta \geq \frac{\sqrt{3}}{2}, \\ 1 - \beta, & \text{if} \quad \beta < \frac{\sqrt{3}}{2}, \end{cases} \tag{10}$$

and $T_{6500} = T_{\rm eff}/6500$ K. The parameter β indicates the location in the accretion disc where the viscous stress impacting the temperature distribution of the disc disappears (Tsygankov et al. 2017). For β of unity, the viscous stress disappears at the magnetospheric radius while for β=0, the stress disappears at a radius much smaller than the magnetospheric radius (Tsygankov et al. 2017). Assuming that the viscous stress disappears at the magnetospheric radius (i.e. β=1) and using $T_{\rm eff} = 6500$ K, the threshold $L_{\rm cold,acc}$ is estimated to be $\sim 4.4 \times 10^{34}$ erg s^{-1} which is shown by a dotted horizontal line in Fig. 12(a) and (b). Interestingly, $L_{\rm cold,acc}$ is higher by a factor of about 4 than $L_{\rm cold}$ and using the more accurate threshold for accretion to proceed from a cold (non-ionised) disc, the estimated luminosities of the source lie below this threshold suggesting that accretion is likely mediated through a cold disc during the prolonged low luminosity period from 2018 December until 2024 February. However, it seems that during the period 2005 April 6 (MJD 53466) until 2010 March 15 (MJD 55270.9), the pulsar was in a low luminosity state and likely not accreting from a cold disc for most of the time. Accretion from a cold disc has been suggested to occur during periods in between outbursts in GRO J1008-57 (lasting for about 200 d Tsygankov et al. 2017). In GX 304-1, this phenomenon has been observed in between Type I outbursts (lasting a few tens of days) and also after the cessation of regular outbursts (lasting for about 400 d Escorial et al. 2018). The prolonged low-luminosity state (spanning a duration of about 5 yr as shown in Fig. 12) powered by accretion from a cold disc in GX 304-1 might be the longest manifestation of this phenomenon reported in any accreting pulsar.

4.5 Accretion from stellar wind

The companion stars in BeXRB systems contain massive stars and it is likely that accretion may proceed directly via the stellar wind. The companion star in GX 304-1 belongs to the B2V class (Mason

https://doi.org/10.1017/pasa.2025.12 Published online by Cambridge University Press

et al. 1978; Thomas et al. 1979; Parkes et al. 1980) which have typical terminal wind velocities (v_w) of ~ 800 km s^{-1} and mass-loss rates of about 10^{-8} M$_\odot$ yr^{-1} (Prinja 1989; Vink, de Koter, & Lamers 2000). Assuming that the gravitational potential energy of the captured stellar wind by the neutron star is entirely converted into X-rays, the X-ray luminosity ($L_{\rm wind}$) is given by Reig & Zezas (2018),

$$L_{\rm wind} \approx 4.7 \times 10^{37} M_{1.4}^{3}\, R_6^{-1}\, M_*^{-2/3}\, P_{\rm orb}^{-4/3}\, \dot{M}_{-6}\, v_{\rm w,8}^{-4}\ {\rm erg\ s^{-1}}, \quad (11)$$

where M_* is the mass of the companion star in solar masses, $P_{\rm orb}$ is the orbital period of the binary in days while $\dot{M}$ and v_w are expressed in units of 10^{-6}M$_\odot$ yr^{-1} and 10^{-8}cm s^{-1}, respectively. Using M_*=9.9 M$_\odot$ (Sugizaki et al. 2015), $v_w \sim 800$ km s^{-1}, $\dot{M} \sim 10^{-8}$M$_\odot$ yr^{-1} for B2V type stars (Prinja 1989; Vink et al. 2000), $P_{\rm orb}$ ~132.2 d (Sugizaki et al. 2015), $M = 10$ M$_\odot$, and $R = 10$ km, the estimated X-ray luminosity from the stellar wind is $\sim 4 \times 10^{32}$ erg s^{-1}. The estimated $L_{\rm wind}$ is lower by about a factor of 15–70 than the range of luminosities of the pulsar shown in Fig. 12(b). The estimated X-ray luminosity during the low state from *XMM-Newton* and *NuStar* observations is $\sim 2.5 \times 10^{33}$ erg s^{-1} in the 0.5–10 keV energy band and $\sim 3.6 \times 10^{33}$ erg s^{-1} in the 3–20 keV energy band, respectively, which are an order of magnitude higher than that can be powered solely by wind accretion. Thus, accretion from the stellar wind emanating from the Be star alone cannot explain the observed long-term low luminosity regime observed in this pulsar, and it is possible that other favourable accretion mechanisms such as accretion through a cold (non-ionised) disc may operate simultaneously.

4.6 Origin of soft excess in the spectra

The hot BB excess ($kT_{\rm BB} >\sim 1$ keV) detected in GX 304-1 is similar to those detected in other BeXRBs RX J0440.9+4431 (La Palombara et al. 2012), RX J0146.9+6121 (La Palombara & Mereghetti 2006), 4U 0352+309 (Coburn et al. 2001; La Palombara & Mereghetti 2007), RX J1037.5-5647 (Reig & Roche 1999; La Palombara et al. 2009), 3A 0535+262 (Mukherjee & Paul 2005), 4U 2206+54 (Masetti 2004; Torrejón et al. 2004; Reig et al. 2009), SAX J2103.5+4545 (Inam et al. 2004), and SXP 1062 (Hénault-Brunet et al. 2012; González-Galán et al. 2018). These BeXRBs have long pulse periods ($P > 100$ s) and the hot BB excess were detected during low luminosity states ($\leq 5 \times 10^{35}$ erg s^{-1}) in these pulsars (La Palombara et al. 2012). The spin period of GX 304-1 is about 275 s and the inferred luminosity during low states is $\sim 2.5 \times 10^{33}$ and $\sim 3.6 \times 10^{33}$ erg s^{-1} from *XMM-Newton* and *NuStar* observations, respectively, which suggests that GX 304-1 also belongs to this category of BeXRBs showing a soft X-ray excess.

It has been shown that in the low luminosity accretion powered pulsars ($L_{\rm X} \leq 10^{36}$ erg s^{-1}), the thermal component can be attributed to either emission by photo-ionised or collisionally heated diffuse gas or thermal emission from the surface of the neutron star (Hickox, Narayan, & Kallman 2004). Assuming that the soft excess comes from the surface of the neutron star, the size of the emission region can be estimated using $R_{\rm col} \sim R_{\rm NS}\,(R_{\rm NS}/R_m)^{0.5}$ (Hickox et al. 2004), where $R_{\rm col}$ is the radius of the accretion column and R_m is the magnetospheric radius. The magnetospheric radius is given by (Campana et al. 1998),

$$R_m = 2 \times 10^{7}\, \dot{M}_{15}^{-2/7}\, B_9^{4/7}\, M_{1.4}^{-1/7}\, R_6^{12/7}\ {\rm cm}, \quad (12)$$

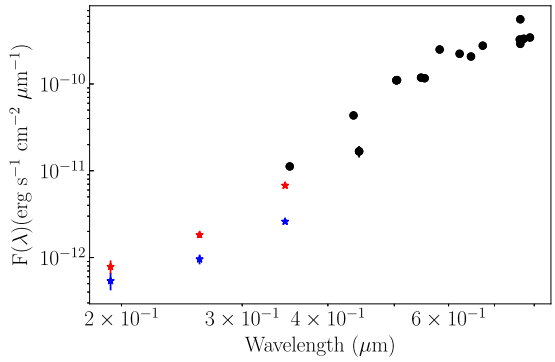

Figure 13. Spectral energy distribution for the companion star of GX 304-1. The black-filled circles show data taken from literature using the *Gaia* (Prusti et al. 2016; Brown et al. 2021) and *TESS* (Stassun et al. 2019) observations and are obtained from the Vizier database (Ochsenbein et al. 2000). The blue and red stars show data from the *Swift*/UVOT in U, UW1 and UW2 filters obtained during the quiescent state just before the regular X-ray outbursts began from the source (around MJD 55268) and that during the beginning of outbursts (around MJD 55550), respectively.

where $\dot{M}$ is the accretion rate (in units of 10^{15} g s^{-1}), B, M and R are the magnetic field, mass and radius of the neutron star, respectively. Using $L_X \sim 5 \times 10^{33}$ erg s^{-1}, $M = 1.4$ M$_\odot$ and $R = 10$ km, the accretion rate is estimated to be $\sim 2.7 \times 10^{13}$ g s^{-1}. Using $B \sim 4.7 \times 10^{12}$ G (Yamamoto et al. 2011a), the magnetospheric radius is estimated to $\sim 7 \times 10^{9}$cm. The estimated radius of the accretion column (which is an estimate of the expected size of the polar cap) is R$_{\rm col} \sim 120$ m which is remarkably similar to the estimated black body emitting radius of about 100–110 m. This suggests that the observed blackbody emission emanates from the polar cap of the neutron star.

4.7 Exploring spectral energy distribution of the companion star

We searched the literature for photometric detection of the companion star at other wavelengths using the catalogues available in the VizieR database (Ochsenbein, Bauer, & Marcout 2000). The catalogue entries using the *Gaia* (Prusti et al. 2016; Brown et al. 2021) and *TESS* (Stassun et al. 2019) observations were taken within 5″ of the source position. The spectral energy distribution (SED) of the companion star is shown in Fig. 13 plotted along with the *Swift*/UVOT estimated fluxes in the U, UW1, and UW2 filters. We have shown the UVOT fluxes obtained during the quiescent state just before the regular X-ray outbursts began from the source (around MJD 55268) and that during the beginning of outbursts (around MJD 55550). There is an indication of UV excess from the companion star when X-ray outbursts were detected from the neutron star compared to the time when the source was in a quiescent phase. The detailed SED modelling of the companion star is beyond the scope of this work.

5. Conclusions

We presented the timing and spectral studies of GX 304-1 using *NuStar* and *XMM-Newton* observations during low state. Pulsations are detected during the low state indicating that the low X-ray luminosity is powered by accretion onto the surface of the neutron star. We construct the long-term spin history of the pulsar and find that the pulsar switched from a long-term spin-up to a spin-down trend during a low luminosity state of the pulsar.

https://doi.org/10.1017/pasa.2025.12 Published online by Cambridge University Press

The long-term photometric observations of the companion star suggest a possible decrease in its recent activity and lack of mass ejection events which trigger X-ray outbursts in this binary. The pulsar shows a prolonged low luminosity regime ($L_X \sim 10^{34}$ erg s^{-1}) spanning nearly five years since 2018 December. The ultraviolet signatures of the companion star precedes the onset of X-ray outbursts in this source by about half a year and does not show any marked variation during the prolonged long-term quiescent state. We explore plausible mechanisms to explain the long-term spin-down and low luminosity manifestation in this pulsar. We detect soft X-ray excess in the spectra which can be attributed to thermal emission from the polar cap of the neutron star. Simultaneous X-ray, optical and ultraviolet monitoring observations of the binary are required to better understand the mechanisms of long-term spin-down, mass-loss dynamics from the companion star and accretion vagaries in this pulsar.

Acknowledgement. We are thankful to the reviewer for making constructive suggestions that improved the presentation of this paper. This paper is dedicated to my mentor P. C. Agrawal who introduced me to the fascinating world of X-ray binaries. ADC thanks Katja Pottschmidt for helpful suggestions regarding the *NuStar* background. ADC thanks Bryan Irby for many prompt suggestions regarding an installation bug in the latest version of the HEASOFT package (ver 6.34). This research has made use of data from the *NuStar* mission, a project led by the California Institute of Technology, managed by the Jet Propulsion Laboratory, and funded by the National Aeronautics and Space Administration. Data analysis was performed using the *NuStar* Data Analysis Software (NUSTARDAS), jointly developed by the ASI Science Data Center (SSDC, Italy) and the California Institute of Technology (USA). This research is based on observations obtained with *XMM-Newton*, an ESA science mission with instruments and contributions directly funded by ESA Member States and NASA. We acknowledge the use of public data from the *Swift* data archive. This research has made use of software provided by the High Energy Astrophysics Science Archive Research Center (HEASARC), which is a service of the Astrophysics Science Division at NASA/GSFC and the High Energy Astrophysics Division of the Smithsonian Astrophysical Observatory. This research has made use of the *MAXI* (Matsuoka et al. 2009) light curve provided by RIKEN, JAXA, and the *MAXI* team. This research has also made use of the *FERMI*/GBM (Meegan et al. 2009) pulsar spin evolution history provided by the *FERMI* team. This research has made use of the *Swift*/BAT (Krimm et al. 2013) light curve provided by the *Swift* team. This research has made use of photometric observations of V850 Cen from ASAS-SN light curves (Shappee et al. 2014; Kochanek et al. 2017). We acknowledge with thanks the variable star observations from the AAVSO International Database contributed by observers worldwide and used in this research. This work has made use of data from the European Space Agency (ESA) mission *Gaia* (https://www.cosmos.esa.int/gaia), processed by the *Gaia* Data Processing and Analysis Consortium (DPAC, https://www.cosmos.esa.int/web/gaia/dpac/consortium). Funding for the DPAC has been provided by national institutions, in particular the institutions participating in the *Gaia* Multilateral Agreement. This research has made use of the SIMBAD astronomical database (Wenger et al. 2000) and NASA's Astrophysics Data System. This research has made use of Astropy (Astropy Collaboration et al. 2013; Astropy Collaboration et al. 2018), Numpy (Harris et al. 2020) and Matplotlib (Hunter 2007) packages. ADC acknowledges support from ARIES through post-doctoral fellowship (AO/RA/2023/1197).

Data availability statement. The *NuStar*, *XMM-Newton* and *Swift*/XRT data used in this research are available for download from the HEASARC (https://heasarc.gsfc.nasa.gov/docs/archive.html). The *FERMI*/GBM pulsar spin evolution history for GX 304-1 provided by the *FERMI* team is available at https://gammaray.nsstc.nasa.gov/gbm/science/pulsars/lightcurves/gx304m1.html. The *Swift*/BAT light curve is available at https://swift.gsfc.nasa.gov/results/transients/weak/GX304-1/. The *MAXI* light curve is publicly available at http://maxi.riken.jp/star_data/J1301-616/J1301-616.html. The photometric observations of V850 Cen are available at https://asas-sn.osu.edu/.

References

Arnaud, K. 1996, in ASP Conf. Ser. 101, Vol. 17, Astronomical Data Analysis Software and Systems V, ed. G. H. Jacoby, & J. Barnes (San Francisco, CA: ASP), https://ui.adsabs.harvard.edu/abs/1996ASPC..101...17A/abstract
Astropy Collaboration, et al. 2013, A&A, 558, A33, https://doi.org/10.1051/0004-6361/201322068
Astropy Collaboration, et al. 2018, AJ, 156, 123, https://doi.org/10.3847/1538-3881/aabc4f
Bildsten, L., et al. 1997, ApJS, 113, 367, https://doi.org/10.1086/313060
Bradt, H., et al. 1977, Natur, 269, 21, https://doi.org/10.1038/269021a0
Brown, A. G., et al. 2021, A&A, 649, A1, https://doi.org/10.1051/0004-6361/202039657
Burrows, D. N., et al. 2005, SSR, 120, 165, https://doi.org/10.1007/s11214-005-5097-2
Caballero-Garca, M. D., et al. 2016, A&A, 589, A9, https://doi.org/10.1051/0004-6361/201526849
Camero-Arranz, A., Finger, M., Ikhsanov, N., Wilson-Hodge, C., & Beklen, E. 2009, ApJ, 708, 1500, https://doi.org/10.1088/0004-637x/708/2/1500
Campana, S., Colpi, M., Mereghetti, S., Stella, L., & Tavani, M. 1998, A&A Rev, 8, 279, https://doi.org/10.1007/s001590050012
Campana, S., et al. 2001, ApJ, 561, 924, https://doi.org/10.1086/323317
Chakrabarty, D., et al. 1997, ApJL, 481, L101, https://doi.org/10.1086/310666
Chandra, A. D., Roy, J., & Agrawal, P. 2023, RAA, 23, 045003, https://doi.org/10.1088/1674-4527/acb980
Chandra, A. D., Roy, J., Agrawal, P., & Choudhury, M. 2020, MNRAS, 495, 2664, https://doi.org/10.1093/mnras/staa1041
Chandra, A. D., Roy, J., Agrawal, P., & Choudhury, M. 2021, MNRAS, 508, 4429, https://doi.org/10.1093/mnras/stab2382
Christodoulou, D., Kazanas, D., & Laycock, S. 2016, arXiv preprint arXiv:1606.07096, https://doi.org/10.48550/arXiv.1606.07096
Coburn, W., et al. 2001, ApJ, 552, 738, https://doi.org/10.1086/320565
Coe, M. J., et al. 2024, MNRAS, 528, 7115, https://doi.org/10.1093/mnras/stae495
Corbet, R., Mason, K., Cordova, F., Branduardi-Raymont, G., & Parmar, A. 1985, MNRAS, 212, 565, https://doi.org/10.1093/mnras/212.3.565
Corbet, R., et al. 1986, MNRAS (ISSN 0035-8711), 221, 961. SERC-supported research., 221, 961, https://doi.org/10.1093/mnras/221.4.961
Devasia, J., James, M., Paul, B., & Indulekha, K. 2011, MNRAS, 417, 348, https://doi.org/10.1111/j.1365-2966.2011.19269.x
Escorial, A. R., van den Eijnden, J., & Wijnands, R. 2018, A&A, 620, L13, https://doi.org/10.1051/0004-6361/201834572
Evans, P., et al. 2009, MNRAS, 397, 1177, https://doi.org/10.1111/j.1365-2966.2009.14913.x
Fritz, S., et al. 2006, A&A, 458, 885, https://doi.org/10.1051/0004-6361:20065557
Gehrels, N., et al. 2004, ApJ, 611, 1005, https://doi.org/10.1063/1.1810924
Ghosh, P., & Lamb, F. 1978, ApJ, 223, L83, https://doi.org/10.1086/182734
Ghosh, P., & Lamb, F. 1979, ApJ, 234, 296, https://doi.org/10.1086/157498
Giacconi, R., et al. 1974, ApJS, 27, 37, https://doi.org/10.1086/190288
González-Galán, A., et al. 2012, A&A, 537, A66, https://doi.org/10.1051/0004-6361/201117893
González-Galán, A., et al. 2018, MNRAS, 475, 2809, https://doi.org/10.1093/mnras/stx3127
Gupta, S., Naik, S., & Jaisawal, G. K. 2019, MNRAS, 490, 2458, https://doi.org/10.1093/mnras/stz2795
Haefner, R. 1988, IBVS, 3260, https://ui.adsabs.harvard.edu/abs/1988IBVS.3260....1H/abstract
Harris, C. R., et al. 2020, Natur, 585, 357, https://doi.org/10.1038/s41586-020-2649-2

Harrison, F. A., et al. 2013, ApJ, 770, 103, https://doi.org/10.1088/0004-637X/770/2/103
Hénault-Brunet, V., et al. 2012, MNRASL, 420, L13, https://doi.org/10.1111/j.1745-3933.2011.01183.x
HI4PI Collaboration, et al. 2016, A&A, 594, A116, https://doi.org/10.1051/0004-6361/201629178
Hickox, R., Narayan, R., & Kallman, T. 2004, ApJ, 614, 881, https://doi.org/10.1086/423928
Huckle, H., et al. 1977, MNRAS, 180, 21P, https://doi.org/10.1093/mnras/180.1.21p
Hunter, J. D. 2007, CSE, 9, 90, https://doi.org/10.1109/mcse.2007.55
Illarionov, A., & Sunyaev, R. 1975, A&A, 39, 185, https://ui.adsabs.harvard.edu/abs/1975A A. . ..39.185I
Inam, S., Baykal, A., Swank, J., & Stark, M. 2004, ApJ, 616, 463, https://doi.org/10.1086/424825
Inam, S., Şahiner, Ş., & Baykal, A. 2009, MNRAS, 395, 1015, https://doi.org/10.1111/j.1365-2966.2009.14596.x
Jaisawal, G. K., Naik, S., & Epili, P. 2016, MNRAS, 457, 2749, https://doi.org/10.1093/mnras/stw085
Jansen, F., et al. 2001, A&A, 365, L1, https://doi.org/10.1051/0004-6361:20000036
Kennea, J., et al. 2020, MNRASL, 499, L41, https://doi.org/10.1093/mnrasl/slaa154
Klochkov, D., et al. 2012, A&A, 542, L28, https://doi.org/10.1051/0004-6361/201219385
Klus, H., Ho, W. C., Coe, M. J., Corbet, R. H., & Townsend, L. J. 2014, MNRAS, 437, 3863, https://doi.org/10.1093/mnras/stt2192
Kluźniak, W., & Rappaport, S. 2007, ApJ, 671, 1990, https://doi.org/10.1086/522954
Kochanek, C., et al. 2017, PASP, 129, 104502, https://doi.org/10.1088/1538-3873/aa80d9
Krimm, H., et al. 2010, ATel, 2538, 1
Krimm, H. A., et al. 2013, ApJS, 209, 14, https://doi.org/10.1088/0067-0049/209/1/14
Kühnel, M., et al. 2010, ATel, 3087, 1
La Palombara, N., & Mereghetti, S. 2006, A&A, 455, 283, https://doi.org/10.1051/0004-6361:20065107
La Palombara, N., & Mereghetti, S. 2007, A&A, 474, 137, https://doi.org/10.1051/0004-6361:20077970
La Palombara, N., Sidoli, L., Esposito, P., Tiengo, A., & Mereghetti, S. 2009, A&A, 505, 947, https://doi.org/10.1051/0004-6361/200912538
La Palombara, N., Sidoli, L., Esposito, P., Tiengo, A., & Mereghetti, S. 2012, A&A, 539, A82, https://doi.org/10.1051/0004-6361/201118221
Leahy, D., et al. 1983, ApJ, 266, 160, https://doi.org/10.1086/160766
Liu, W., et al. 2023, arXiv preprint arXiv:2311.13844, https://doi.org/10.48550/arXiv.2311.13844
Makishima, K., et al. 1988, Natur, 333, 746, https://doi.org/10.1038/333746a0
Malacaria, C., et al. 2020, ApJ, 896, 90, https://doi.org/10.3847/1538-4357/ab855c
Malacaria, C., Klochkov, D., Santangelo, A., & Staubert, R. 2015, A&A, 581, A121, https://doi.org/10.1051/0004-6361/201526417
Malacaria, C., et al. 2017, A&A, 603, A24, https://doi.org/10.1051/0004-6361/201730538
Manousakis, A., et al. 2008, ATel, 1613, 1
Masetti, N., et al. 2004, A&A, 423, 311, https://doi.org/10.1051/0004-6361:20040273
Mason, K., Murdin, P., Parkes, G., & Visvanathan, N. 1978, MNRAS, 184, 45P, https://doi.org/10.1093/mnras/184.1.45p
Matsuoka, M., et al. 2009, PASJ, 61, 999, https://doi.org/10.1093/pasj/61.5.999
Maurer, G. S., Johnson, W. N., Kurfess, J. D., & Strickman, M. S. 1982, ApJ, 254, 271. Navy-NASA-supported research., 254, 271, https://doi.org/10.1086/159730
McClintock, J. E., Rappaport, S. A., Nugent, J. J., & Li, F. K. 1977, Ap, 216, L15, https://doi.org/10.1086/182499
McClintock, J. E., Ricker, G. R., & Lewin, W. H. 1971, ApJ, 166, L73, https://doi.org/10.1086/180742
Meegan, C., et al. 2009, ApJ, 702, 791, https://doi.org/10.1088/0004-637X/702/1/791
Menzies, J. 1981, MNRAS, 195, 67P, https://doi.org/10.1093/mnras/195.1.67p
Mihara, T., et al. 2010, ATel, 2779, 1
Miyasaka, H., et al. 2013, ApJ, 775, 65, https://doi.org/10.1088/0004-637x/775/1/65
Mukherjee, U., & Paul, B. 2005, A&A, 431, 667, https://doi.org/10.1051/0004-6361:20041665
Nagase, F. 1989, PASJ, 41, 1, https://ui.adsabs.harvard.edu/abs/1989PASJ...41....1N/abstract
Nakajima, M., et al. 2010, ATel, 3075, 1
Nakajima, M., et al. 2016a, ATel, 9064, 1
Nakajima, M., et al. 2016b, ATel, 8592, 1
Negueruela, I., et al. 1997, MNRAS, 284, 859, https://doi.org/10.1093/mnras/284.4.859
Ochsenbein, F., Bauer, P., & Marcout, J. 2000, A&AS, 143, 23, https://doi.org/10.1051/aas:2000169
Parkes, G., Murdin, P., & Mason, K. 1980, MNRAS, 190, 537, https://doi.org/10.1093/mnras/190.3.537
Pietsch, W., Oegelman, H., Kahabka, P., Collmar, W., & Gottwald, M. 1986, A&A, 163, 93, https://ui.adsabs.harvard.edu/abs/1986AA...163...93P/abstract
Postnov, K., et al. 2015, MNRAS, 446, 1013, https://doi.org/10.1093/mnras/stu2155
Priedhorsky, W., & Terrell, J. 1983, ApJ, Part 1 (ISSN 0004-637X). Research sponsored by the US Department of Energy, 273, 709, https://doi.org/10.1086/161406
Pringle, J., & Rees, M. 1972, A&A, 21, 1, https://ui.adsabs.harvard.edu/abs/1972A%26A....21....1P/abstract
Prinja, R. K. 1989, MNRAS, 241, 721, https://doi.org/10.1093/mnras/241.4.721
Prusti, T., et al. 2016, A&A, 595, A1, https://doi.org/10.1051/0004-6361/201629272
Reig, P., Larionov, V., Negueruela, I., Arkharov, A., & Kudryavtseva, N. 2007, A&A, 462, 1081, https://doi.org/10.1051/0004-6361:20066217
Reig, P., & Roche, P. 1999, MNRAS, 306, 100, https://doi.org/10.1046/j.1365-8711.1999.02473.x
Reig, P., et al. 2009, A&A, 494, 1073, https://doi.org/10.1051/0004-6361:200810950
Reig, P., & Zezas, A. 2018, A&A, 613, A52, https://doi.org/10.1051/0004-6361/201732533
Roming, P. W., et al. 2005, SSR, 120, 95, https://doi.org/10.1007/s11214-005-5095-4
Rouco Escorial, A., & Wijnands, R. 2016, ATel, 9101, 1
Sguera, V., & Sidoli, L. 2016, ATel, 9067, 1
Shakura, N., Postnov, K., Kochetkova, A., & Hjalmarsdotter, L. 2012, MNRAS, 420, 216, https://doi.org/10.1111/j.1365-2966.2011.20026.x
Shakura, N., Postnov, K., Kochetkova, A. Y., & Hjalmarsdotter, L. 2014, in EPJ Web of Conferences, Vol. 64, EDP Sciences, 02001, https://doi.org/10.1051/epjconf/20136402001
Shappee, B. J., et al. 2014, ApJ, 788, 48, https://doi.org/10.1088/0004-637x/788/1/48
Stassun, K. G., et al. 2019, AJ, 158, 138, https://doi.org/10.3847/1538-3881/ab3467
Strüder, L., et al. 2001, A&A, 365, L18, https://doi.org/10.1051/0004-6361:20000066
Sugizaki, M., Mihara, T., Nakajima, M., & Makishima, K. 2017, PASJ, 69, 100, https://doi.org/10.1093/pasj/psx119
Sugizaki, M., Yamamoto, T., Mihara, T., Nakajima, M., & Makishima, K. 2015, PASJ, 67, 73, https://doi.org/10.1093/pasj/psv039
Thomas, R., Morton, D., & Murdin, P. 1979, MNRAS, 188, 19, https://doi.org/10.1093/mnras/188.1.19
Torrejón, J. M., Kreykenbohm, I., Orr, A., Titarchuk, L., & Negueruela, I. 2004, A&A, 423, 301, https://doi.org/10.1051/0004-6361:20035743
Townsend, L., et al. 2017, MNRAS, 471, 3878, https://doi.org/10.1093/mnras/stx1865

Treuz, S., Doroshenko, V., Santangelo, A., & Staubert, R. 2018, arXiv preprint arXiv:1806.11397, https://doi.org/10.48550/arXiv.1806.11397
Tsygankov, S., et al. 2016, A&A, 593, A16, https://doi.org/10.1051/0004-6361/201628236
Tsygankov, S., et al. 2017, A&A, 608, A17, https://doi.org/10.1051/0004-6361/201630248
Tsygankov, S. S., et al. 2019, MNRASL, 483, L144, https://doi.org/10.1093/mnrasl/sly236
Turner, M. J., et al. 2001, A&A, 365, L27, https://doi.org/10.1051/0004-6361:20000087
Usui, R., et al. 2012, PASJ, 64, 79, https://doi.org/10.1093/pasj/64.4.79
Vink, J. S., de Koter, A., & Lamers, H. J. 2000, arXiv preprint astro-ph/0008183, https://doi.org/10.48550/arXiv.astro-ph/0008183
Wang, Y.-M. 1996, ApJ, 465, L111, https://doi.org/10.1086/310150
Wenger, M., et al. 2000, A&AS, 143, 9, https://doi.org/10.1051/aas:2000332
White, N., Swank, J., & Holt, S. 1983, ApJ, Part 1 (ISSN 0004-637X), 270, 711, https://ui.adsabs.harvard.edu/abs/1983ApJ...270..711W/abstract
Wilms, J., Allen, A., & McCray, R. 2000, ApJ, 542, 914, https://doi.org/10.1086/317016
Yamamoto, T., et al. 2011a, PASJ, 63, S751, https://doi.org/10.1093/pasj/63.sp3.s751
Yamamoto, T., et al. 2009, ATel, 2297, 1
Yamamoto, T., et al. 2011b, ATel, 3309, 1
Yamamoto, T., et al. 2011c, ATel, 3624, 1
Yamamoto, T., et al. 2012, ATel, 3856, 1

https://doi.org/10.1017/pasa.2025.12 Published online by Cambridge University Press

Appendix

Appendix A. Additional tables

Table A1. *Swift*/XRT observations of GX 304-1 spanning the duration 2005 April 6 (MJD 53466) until 2010 March 15 (MJD 55270.9).

S. no.	Obs Id	Date	Exposure	XRT count rate (XCR)	$\frac{XCR}{XCR_{fixed}}$ [a]	Luminosity[b]
		MJD	ks	counts s^{-1}		10^{34} erg s^{-1}
1	35072001	53466.01	3.50	0.552 ± 0.021	4.18	5.20 ± 0.2
2	35072002	53998.05	4.14	1.229 ± 0.023	9.31	11.57 ± 0.22
3	35072003	53999.05	8.02	1.093 ± 0.016	8.28	10.29 ± 0.15
4	35072004	54091.85	4.56	0.885 ± 0.019	6.70	8.33 ± 0.18
5	35072005	55263.23	1.14	1.19 ± 0.06	9.02	11.20 ± 0.56
6	35072006	55263.69	1.16	0.537 ± 0.024	4.07	5.06 ± 0.23
7	35072007	55264.23	1.17	0.541 ± 0.024	4.10	5.09 ± 0.23
8	35072008	55264.70	1.16	0.546 ± 0.024	4.14	5.14 ± 0.23
9	35072009	55265.25	0.88	0.85 ± 0.03	6.44	8.00 ± 0.28
10	35072010	55265.78	1.00	0.593 ± 0.027	4.49	5.58 ± 0.25
11	35072011	55266.24	1.40	0.543 ± 0.025	4.11	5.11 ± 0.24
12	35072012	55266.78	1.28	0.392 ± 0.02	2.97	3.69 ± 0.19
13	35072013	55267.12	0.85	0.47 ± 0.026	3.56	4.42 ± 0.24
14	35072014	55267.78	1.27	0.551 ± 0.023	4.17	5.19 ± 0.22
15	35072015	55268.25	1.42	0.63 ± 0.023	4.77	5.93 ± 0.22
16	35072016	55268.78	1.27	0.528 ± 0.022	4.00	4.97 ± 0.21
17	35072017	55269.18	1.32	0.491 ± 0.021	3.72	4.62 ± 0.2
18	35072018	55269.93	0.98	0.52 ± 0.026	3.94	4.90 ± 0.24
19	35072019	55270.39	1.21	0.64 ± 0.025	4.85	6.02 ± 0.24
20	35072020	55270.86	1.27	0.613 ± 0.024	4.64	5.77 ± 0.23

Notes: [a]XCR and $XCR_{fixed} = 0.13$ are the XRT count rates for the given epoch in the table and MJD 58272.3 (2018 June 3), respectively.
[b]Luminosity in the 0.5–100 keV energy range from Tsygankov et al. (2019) using a distance of 2.01 kpc (Treuz et al. 2018) scaled using $\frac{XCR}{XCR_{fixed}}$.

Table A2. *Swift*/XRT observations of GX 304-1 spanning the period from 2018 December 17 (MJD 58469) until 2024 February 27 (MJD 60367.8).

S. no.	Obs Id	Date	Exposure	XRT count rate (XCR)	$\frac{XCR}{XCR_{fixed}}$ [a]	Luminosity[b]
		MJD	ks	counts s^{-1}		10^{34} erg s^{-1}
1	00035072138	58469.00	0.78	0.176 ± 0.017	1.33	1.66 ± 0.16
2	00035072139	58483.41	0.66	0.209 ± 0.02	1.58	1.97 ± 0.19
3	00035072140	58497.62	0.99	0.219 ± 0.016	1.66	2.06 ± 0.15
4	00035072142	58514.96	0.98	0.151 ± 0.015	1.14	1.42 ± 0.14
5	00035072144	58528.55	0.58	0.16 ± 0.02	1.21	1.51 ± 0.19
6	00035072145	58539.38	0.91	0.116 ± 0.015	0.88	1.09 ± 0.14
7	00035072146	58553.27	1.09	0.23 ± 0.017	1.74	2.17 ± 0.16
8	00035072147	58567.42	1.04	0.139 ± 0.013	1.05	1.31 ± 0.12
9	00035072148	58581.14	1.12	0.136 ± 0.017	1.03	1.28 ± 0.16
10	00035072150	58643.04	0.90	0.171 ± 0.015	1.30	1.61 ± 0.14
11	00035072151	58650.97	0.80	0.161 ± 0.017	1.22	1.52 ± 0.16
12	00035072152	58657.92	0.90	0.118 ± 0.014	0.89	1.11 ± 0.13
13	00035072153	58664.63	0.47	0.118 ± 0.019	0.89	1.11 ± 0.18
14	00035072154	58671.14	0.91	0.125 ± 0.014	0.95	1.18 ± 0.13

https://doi.org/10.1017/pasa.2025.12 Published online by Cambridge University Press

Table A2. Continued

S. no.	Obs Id	Date	Exposure	XRT count rate (XCR)	$\frac{XCR}{XCR_{fixed}}$ [a]	Luminosity[b]
15	00035072155	58678.04	0.94	0.089 ± 0.012	0.67	0.84 ± 0.01
16	00035072156	58685.08	0.92	0.162 ± 0.015	1.23	1.52 ± 0.14
17	00035072157	58691.51	0.81	0.194 ± 0.022	1.47	1.83 ± 0.21
18	00035072158	58700.16	0.76	0.277 ± 0.022	2.10	2.61 ± 0.21
19	00035072159	58706.47	1.01	0.209 ± 0.016	1.58	1.97 ± 0.15
20	00035072161	58845.96	0.91	0.215 ± 0.017	1.63	2.02 ± 0.16
21	00035072162	58855.47	0.61	0.177 ± 0.02	1.34	1.67 ± 0.19
22	00035072163	58860.24	0.99	0.104 ± 0.015	0.79	0.98 ± 0.01
23	00035072164	58865.95	0.86	0.148 ± 0.016	1.12	1.39 ± 0.15
24	00035072166	58875.98	0.60	0.194 ± 0.022	1.47	1.83 ± 0.21
25	00035072167	58880.03	0.33	0.085 ± 0.029	0.64	0.08 ± 0.03
26	00035072168	58885.22	0.67	0.153 ± 0.021	1.16	1.44 ± 0.2
27	00035072169	59091.29	4.78	0.139 ± 0.006	1.05	1.31 ± 0.06
28	00035072170	59436.08	2.64	0.12 ± 0.009	0.91	1.13 ± 0.08
29	00035072171	60135.96	4.60	0.14 ± 0.006	1.06	1.32 ± 0.06
30	00035072172	60188.77	1.09	0.163 ± 0.026	1.23	1.53 ± 0.24
31	00035072173	60195.64	0.76	0.134 ± 0.015	1.02	1.26 ± 0.14
32	00035072174	60202.44	0.90	0.164 ± 0.015	1.24	1.54 ± 0.14
33	00035072175	60209.11	0.94	0.122 ± 0.014	0.92	1.15 ± 0.13
34	00035072176	60216.11	1.01	0.18 ± 0.024	1.36	1.69 ± 0.23
35	00035072177	60223.97	0.59	0.227 ± 0.028	1.72	2.14 ± 0.26
36	00035072178	60230.17	0.94	0.103 ± 0.013	0.78	0.97 ± 0.01
37	00035072179	60244.51	0.93	0.308 ± 0.026	2.33	2.9 ± 0.24
38	00035072180	60251.84	0.86	0.064 ± 0.011	0.48	0.6 ± 0.01
39	00035072181	60313.84	0.78	0.115 ± 0.015	0.87	1.08 ± 0.14
40	00035072184	60331.45	0.91	0.182 ± 0.017	1.38	1.71 ± 0.16
41	00035072186	60347.88	0.92	0.253 ± 0.019	1.92	2.38 ± 0.18
42	00035072187	60349.99	0.97	0.132 ± 0.019	1.00	1.24 ± 0.18
43	00035072188	60355.13	0.71	0.143 ± 0.017	1.08	1.35 ± 0.16
44	00035072189	60361.38	1.08	0.128 ± 0.014	0.97	1.2 ± 0.13
45	00035072190	60367.84	0.86	0.145 ± 0.015	1.10	1.36 ± 0.14

Notes: [a] XCR and $XCR_{fixed} = 0.13$ are the XRT count rates for the given epoch in the table and MJD 58272.3 (2018 June 3), respectively.
[b] Luminosity in the 0.5–100 keV energy range from Tsygankov et al. (2019) using a distance of 2.01 kpc (Treuz et al. 2018) scaled using $\frac{XCR}{XCR_{fixed}}$.

https://doi.org/10.1017/pasa.2025.12 Published online by Cambridge University Press